

# JGR Atmospheres



# RESEARCH ARTICLE

10.1029/2022JD036714

#### **Key Points:**

- Our paper focuses on the long-term trend and decadal variation of water vapor in the tropical middle atmosphere
- Methane oxidation explains most of the water vapor increases in the upper stratosphere and mesosphere over 1980–1995
- Changes in residual circulation lead to changes in the tropical tropopause temperature, and middle atmospheric water vapor over 1995–2020

# **Supporting Information:**

Supporting Information may be found in the online version of this article.

#### Correspondence to:

W. Yu, wandi.yu@hamptonu.edu

#### Citation:

Yu, W., Garcia, R., Yue, J., Russell, J. III, & Mlynczak, M. (2022). Variability of water vapor in the tropical middle atmosphere observed from satellites and interpreted using SD-WACCM simulations. *Journal of Geophysical Research: Atmospheres*, 127, e2022ID036714. https://doi.org/10.1029/2022JD036714

Received 28 FEB 2022 Accepted 16 JUN 2022

### **Author Contributions:**

**Conceptualization:** Wandi Yu, Rolando Garcia, Jia Yue

Data curation: Wandi Yu Investigation: Wandi Yu, Rolando Garcia, Jia Yue, James Russell, Martin Mlynczak

Methodology: Wandi Yu, Rolando Garcia, Jia Yue, James Russell Software: Wandi Yu

**Supervision:** Rolando Garcia, Jia Yue, James Russell, Martin Mlynczak

© 2022. The Authors.

This is an open access article under the terms of the Creative Commons Attribution-NonCommercial-NoDerivs License, which permits use and distribution in any medium, provided the original work is properly cited, the use is non-commercial and no modifications or adaptations are made.

# Variability of Water Vapor in the Tropical Middle Atmosphere Observed From Satellites and Interpreted Using SD-WACCM Simulations

Wandi Yu<sup>1</sup>, Rolando Garcia<sup>2</sup>, Jia Yue<sup>3,4</sup>, James Russell III<sup>1</sup>, and Martin Mlynczak<sup>5</sup>

<sup>1</sup>Department of Atmospheric and Planetary Sciences, Hampton University, Hampton, VA, USA, <sup>2</sup>Atmospheric Chemistry Observations & Modeling, National Center for Atmospheric Research, Boulder, CO, USA, <sup>3</sup>NASA Goddard Space Flight Center, Greenbelt, MD, USA, <sup>4</sup>Catholic University of America, Washington, DC, USA, <sup>5</sup>NASA Langley Research Center, Hampton, VA, USA

**Abstract** Water vapor in the middle atmosphere plays an essential role in global warming, ozone depletion, and the formation of polar stratospheric and mesospheric clouds. We show that tropical middle atmospheric water vapor simulated with the specified-dynamics version of the Whole Atmosphere Community Climate Model (SD-WACCM) is consistent with changes observed in a merged satellite data set, which encompasses the period 1993–2020. Consistent with previous work, we find no significant trend in the stratosphere in either the observations or the simulation; in the mesosphere, we find a long-term trend of 0.1 ppmv per decade, but only in the observations. We also analyze an SD-WACCM simulation for the longer period 1980–2019 to quantify the contribution of various factors to the decadal variation of middle atmospheric water vapor. Over 1980–1995, the simulated water vapor in the upper stratosphere and mesosphere, averaged zonally and over ±30° latitude, increases by 0.30 ppmv per decade due to increasing methane emissions. After 1995, a significant abrupt decrease of water vapor of 0.37 ppmv per decade and then a gradual increase of 0.33 ppmv per decade result from changes in stratospheric cold point temperature. The cold-point temperature is strongly influenced by the strength of the Brewer-Dobson circulation. The acceleration of the Brewer-Dobson circulation before about 2003 leads to a cooler tropical tropopause and a decrease of water vapor, and the deceleration thereafter leads to corresponding warming of the tropopause and an increase in water vapor.

**Plain Language Summary** Water vapor in the middle atmosphere is important to global warming and ozone depletion. We analyze both satellite data and climate model output to understand its variation in the past four decades. We conclude that there is a slight increasing trend in observed mesospheric water vapor, but no significant trend in stratospheric water vapor. Model simulation results indicate that methane oxidation explains most of the increase of water vapor in the upper stratosphere and mesosphere over 1980–1995. Changes in the meridional circulation of the middle atmosphere lead to changes in the tropical tropopause temperature, which is the main factor that influences middle atmospheric water vapor over 1995–2020.

# 1. Introduction

Water vapor plays an essential role in climate in the whole atmosphere. As a greenhouse gas, it contributes to surface and tropospheric warming and to cooling in the middle and upper atmosphere (Dvortsov & Solomon, 2001; Forster & Shine, 1999, 2002; Maycock et al., 2014; Rind & Lonergan, 1995; Shindell, 2001; Smith et al., 2001; Solomon et al., 2010), and provides a significant positive feedback to increases in well-mixed greenhouse gases (Dessler et al., 2013). It is an important source of the hydroxyl radical, which participates in the catalysis of ozone depletion in the stratosphere (Dvortsov & Solomon, 2001; Evans et al., 1998; Kirk-Davidoff et al., 1999; Shindell, 2001). It also forms polar stratospheric clouds and polar mesospheric clouds (Hervig et al., 2016; Lübken et al., 2018; Russell et al., 2014; Thomas, 2003).

The budget of water vapor in the middle atmosphere has two sources: water vapor entering the stratosphere in the tropical, upwelling branch of the Brewer-Dobson circulation, and water vapor from methane oxidation. In the upper stratosphere and mesosphere, methane oxidizes and 1 mol of methane generates about 2 mol of water vapor (Bates & Nicolet, 1950; Dessler et al., 1994; Flentje et al., 2005; Gunson et al., 1990; Hansen & Robinson, 1989; Jones et al., 1986; le Texier et al., 1988; Noël et al., 2018; Rosenlof, 2002). Previous studies have shown that methane oxidation plays an important role to the water vapor budget at least above 22 km (Hurst et al., 2011;

YU ET AL. 1 of 18



Validation: Wandi Yu, Rolando Garcia Writing – original draft: Wandi Yu Writing – review & editing: Rolando Garcia, Jia Yue, James Russell, Martin Mlynczak Oman et al., 2008), but changes in methane are not enough to explain the overall water vapor variation (Kley et al., 2000; Randel et al., 2004; Rosenlof et al., 2001).

Most of the water vapor in the middle atmosphere enters the stratosphere through the extremely cold tropical tropopause layer, where much of it condenses and is removed by precipitation, such that only a few ppmv of water vapor is present in air parcels that reach the stratosphere (Fueglistaler et al., 2009; Sherwood & Dessler, 2000). Thus, the cold point temperature in the tropical tropopause layer controls how much water vapor can enter the stratosphere directly (Bonazzola & Haynes, 2004; Fueglistaler & Haynes, 2005; Mote et al., 1996; Nedoluha et al., 2013; Randel et al., 2004; Randel & Park, 2019; Sherwood & Dessler, 2000). The physical processes that impact cold point temperature, such as El Niño-Southern Oscillation (ENSO) and the quasi-biennial oscillation (QBO), can therefore influence the water vapor mixing ratio (Garfinkel et al., 2013; Geller et al., 2002; Liu et al., 2019; Oman et al., 2008; Scaife et al., 2003; Tao et al., 2015; Zahn et al., 2014). It has also been argued that deep convection can penetrate the cold point tropopause (Cooney et al., 2021; Johansson et al., 2015; Sherwood et al., 2004), and bring air with high water vapor content to the stratosphere, bypassing the cold point temperature constraint (Dessler et al., 2016; Schoeberl et al., 2014; Schwartz et al., 2013; Wang et al., 2019; Ye et al., 2018; Yu et al., 2020; Zahn et al., 2014).

Because of its importance to the climate, the long-term trend of middle atmospheric water vapor has long been studied. Many of the satellite observations and model simulations suggest that there is no significant trend in the past several decades (Dessler et al., 2014; Froidevaux et al., 2019; Hegglin et al., 2014). However, Frost Point Hygrometer (FPH) measurements over Boulder, launched since 1980, show a significant positive trend in lower stratospheric water vapor (Hurst et al., 2011; Lossow et al., 2018). Meanwhile, almost all climate models predict that middle atmospheric water vapor will increase by 0.5–1 ppmv due to an increase of the cold point temperature over the 21st century (Gettelman et al., 2009, 2010).

When considering the decadal scale, water vapor in the middle atmosphere shows significant changes of varying sign. For example, before 1998, a positive trend is observed (e.g., Dvortsov & Solomon, 2001). Between about 1998 and 2003, there is a large drop in the water vapor mixing ratio; the proposed reasons for this large change include acceleration of the Brewer-Dobson circulation, ENSO, and changing phase of the QBO (Brinkop et al., 2016; Ding & Fu, 2018; Garfinkel et al., 2018, 2020; Randel et al., 2006; Rosenlof & Reid, 2008). After 2003, the water vapor mixing ratio in the middle atmosphere increases again. During these relatively short periods, the trend of water vapor in the middle atmosphere can be as large as 5% per decade, which is too large to be explained merely by methane oxidation (Fernando et al., 2020; Froidevaux et al., 2019; Yue et al., 2019).

Understanding the drivers of past water vapor long-term trends and decadal variations may help improve the prediction of future trends. There are still debates regarding (a) whether the middle atmospheric water vapor trend over the past few decades is significant; (b) how important are the cold point temperature and methane emissions for driving significant decadal-scale increasing and decreasing variations; and (c) what is the driver for changes of the cold point temperature. The analysis in this paper is based on data from satellite observations and simulations made with the specified dynamics version of the Whole Atmospheric Community Climate Model, version 6 (SD-WACCM6), which is described below. We separate the water vapor in the middle atmosphere into its different sources (methane oxidation, cold point temperature, and deep convection), and quantify the contribution from each source and how these contributions change during different periods. We finally look closely into how anthropogenic activity influences changes in each source, which provides insights for prediction of water vapor based on future human activities.

# 2. Data

# 2.1. Satellite Data

The Sounding of the Atmosphere using Broadband Emission Radiometry (SABER) instrument on the Thermosphere-Ionosphere-Mesosphere Energetics and Dynamics (TIMED) satellite was launched on 7 December 2001 and has provided measurements since January of 2002. The SABER instrument is described in detail by Russell et al. (1999). We use the v2.07 SABER water vapor product, which is retrieved from the 6.8 µm channel and screened to discard observations over 12 ppmv (Rong et al., 2019). SABER observes two local times every day, and covers 83°N–83°S, switching from 53°N–83°S to 83°N–53°S about every 60 days due to satellite yaw maneuvers that prevent the sensor from looking directly at the Sun. The vertical resolution is

YU ET AL. 2 of 18



2 km, and measurements are made from 100 hPa to 0.006 hPa. Local time variation in SABER  $\rm H_2O$  is neglected in our long-term trend study. Tidal variations in  $\rm H_2O$  are important only above 70 km (Rong et al., 2019). The random error of the SABER water vapor product is less than 4% below 60 km, and increases to 30% at 80 km (Rong et al., 2019). The systematic error is 10%-20%. The retrieval of water vapor in the infrared spectral range is heavily dependent on temperature, and the systematic error due to temperature is 20% below 30 km ( $\sim$ 14 hPa) (Remsberg et al., 2008; Rong et al., 2019). During part of the first year after launch there are anomalous water vapor values that appear to be related to changing detector sensitivity due to icing. After May of 2002 the problem was addressed by periodically cycling off the cryocooler to sublimate the ice (see Remsberg et al., 2008, for details). For this reason, and because we have elected to use whole years of data, we use SABER data from 2003 to 2020. We grid the monthly data into 5° latitude and  $10^\circ$  longitude grid boxes.

The Microwave Limb Sounder (MLS) on the Aura satellite was launched on 15 July 2004 (Waters et al., 2006). We use the v5.0 water vapor product of MLS, which is retrieved from the 190-GHz band (Livesey et al., 2020). There are about 3,500 observations per day in the MLS product. They cover 82°N-82°S and 316-0.001 hPa, with a vertical resolution of 1.2-3.6 km below 0.22 hPa and 6-11 km above 0.22 hPa. The random error of the MLS v5.0 water vapor product is 6% in the stratosphere and increases rapidly to as high as 55% at 80 km. The systematic error is 5%-19% (Lambert et al., 2007; Read et al., 2007). We screen the MLS data following the instructions in the data description document (Livesey et al., 2020). One major improvement of the v5.0 data compared to previous versions is that part of the "slow drift" problem in water vapor data is resolved (Hurst et al., 2016; Livesey et al., 2020, 2021). In our study, we use MLS data from 2005 to 2020, and grid the monthly data into 5° latitude and 10° longitude grid boxes.

The Halogen Occultation Experiment (HALOE) on the Upper Atmosphere Research Satellite (UARS) was launched on 12 September 1991 (Russell et al., 1993). We use the v19 level 2 water vapor product, which consists of the solar occultation measurements retrieved from the 6.605 µm band. The HALOE product has about 400 observations per month. They cover 80°N–80°S and 100 hPa – 0.005 hPa, with a vertical resolution of 2 km. The random error of the HALOE water vapor product is 7%–13%, and the systematic error is 19%–24% (Kley et al., 2000). We screen the trip angle problem and cloud contamination events from the HALOE data (http://haloe.gats-inc.com/user\_docs/). The accuracy of HALOE data in 1992 is influenced by the Mount Pinatubo volcanic aerosols, so we use the HALOE data from January 1993 to November 2005 (S. Davis et al., 2016). We also grid the HALOE data into 5° latitude and 10° longitude grid boxes.

# 2.2. Merged Satellite Data

To have an observational data record long enough to cover the low frequency natural variability throughout the middle atmosphere, we merge SABER, MLS, and HALOE into a 28-year data set, 1993–2020. We include HALOE data to extend the temporal coverage of our merged data, and include SABER and MLS data for their accuracy in the mesosphere and stratosphere, respectively.

Our merged data set is constructed from bi-monthly averages of all the data because of a peculiarity of the SABER sampling pattern: In order to avoid looking directly at the sun, SABER must execute periodic yaw maneuvers. Over the course of the SABER mission the yaw cycles drift with respect to local time (LT), such that LT sampling over a single month of SABER observations is not uniform in time, which can introduce spurious trends. The problem can be obviated by averaging the data over complete yaw cycles, since all LT are sampled during each yaw cycle. The duration of a SABER yaw cycle is 60 days, so uniform LT sampling can be ensured by averaging SABER data over 2 months (see Rezac et al., 2018, their Figure 1 and related discussion).

Our merging methodology is similar to previous merging procedures (Froidevaux et al., 2015; Randel & Park, 2019). For each data set, we calculate the deseasonalized water vapor anomalies averaged over 5° latitudinal bands between 30°N and 30°S for each pressure level from 100 hPa to 0.01 hPa, and then merge the data on each pressure level. Due to the sparseness of HALOE sampling, the calculation is done on zonal mean values. We show the calculation at several vertical levels in Figure 1 as an example. We first merge SABER and MLS water vapor anomalies, and then combine the merged SABER and MLS data with the HALOE water vapor anomalies.

When we merge SABER and MLS data during the overlap period between SABER and MLS (2005.01–2020.12), we use the mean value of the water vapor anomaly as the merged result (green solid line in Figure 1). During the early part of the SABER era (2003.01–2004.12), the merged result (green solid line) is the SABER water vapor

YU ET AL. 3 of 18



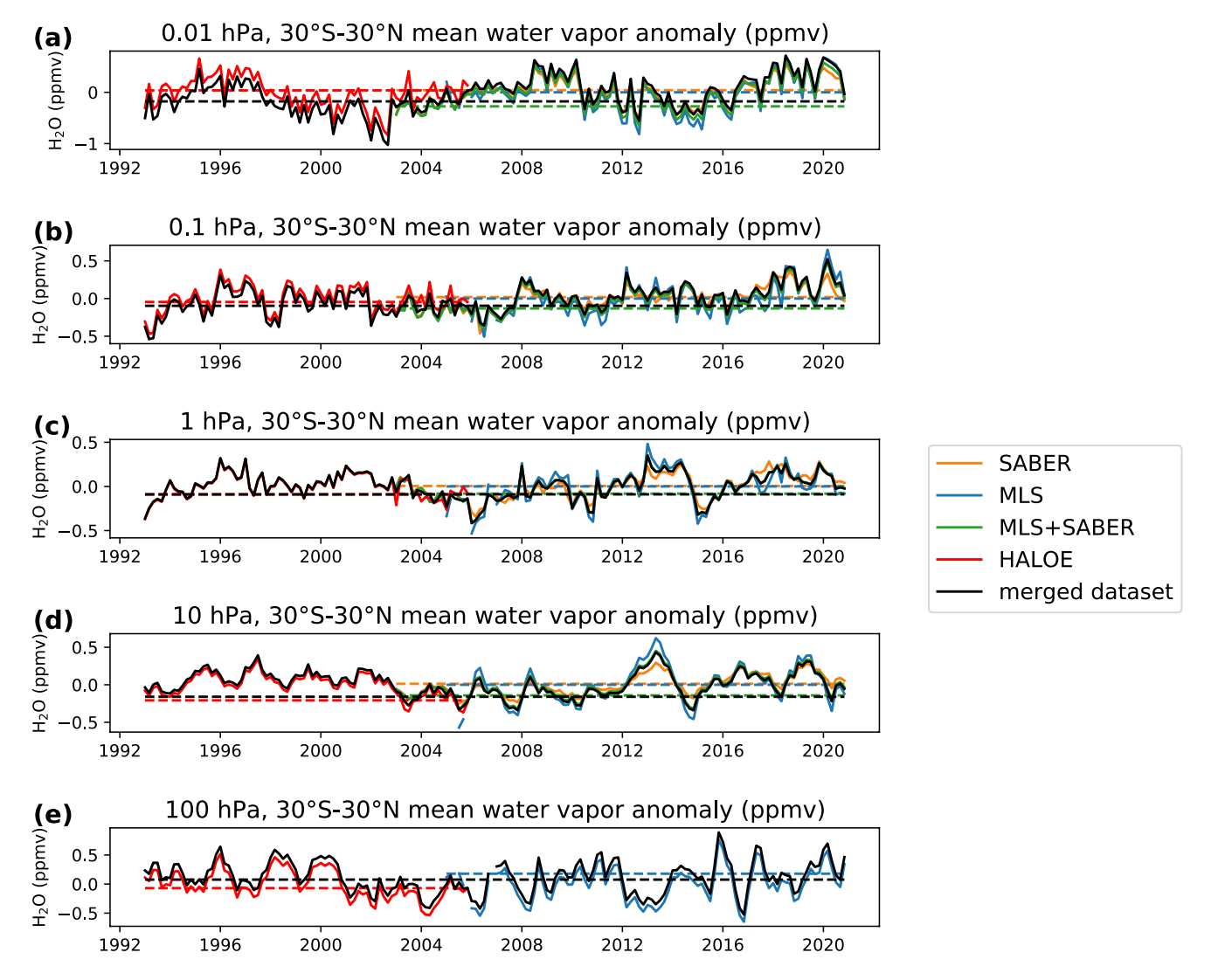


Figure 1. Time series of 30°N–30°S mean deseasonalized water vapor mixing ratio at (a) 0.01 hPa, (b) 0.1 hPa, (c) 1 hPa, (d) 10 hPa, and (e) 100 hPa, observed by Microwave Limb Sounder (MLS) (blue solid line), Sounding of the Atmosphere using Broadband Emission Radiometry (SABER) (orange solid line), and Halogen Occultation Experiment (HALOE) (red solid line), and in the merged MLS + SABER data (green solid line), and the merged MLS + SABER + HALOE data (black line). Dashed lines are the average value of each data set during the overlap period (i.e., 2005.01–2020.12 when merging SABER and MLS data, and 2003.01–2005.11 for HALOE and merged SABER + MLS).

anomalies minus the difference between the mean SABER water vapor anomalies (orange dashed line) and the mean merged result (green dashed line), both averaged during the overlap period.

Next, we merge in HALOE data. During the overlap period between SABER and HALOE (2003.01–2005.11), the merged value of the water vapor anomaly is the weighted mean of 1/3 of the HALOE anomalies plus 2/3 of the merged SABER and MLS anomalies (black solid line). Thus, every data source is given the same weight when merging. During the rest of the HALOE era (1993.01–2002.12), the merged result is the HALOE water vapor anomalies minus the difference between mean HALOE water vapor anomalies (red dashed line) and mean merged result (black dashed line in Figure 1), both averaged during the overlap period.

Below 14 hPa (see Figure 1e as an example), where the systematic error of the SABER water vapor is large, we only merge MLS and HALOE data. During the overlap period between MLS and HALOE (2005.01–2005.11), the merged value of water vapor anomaly is the weighted mean of half of the HALOE anomalies plus half of the MLS anomalies (black solid line). During the rest of the HALOE era (1993.01–2004.12), the merged result is the HALOE water vapor anomalies minus the difference between the mean HALOE water vapor anomalies (red

YU ET AL. 4 of 18



dashed line) and the mean merged result (black dashed line in Figure 1), both averaged during the overlap period. During the rest of the MLS era (2005.12–2020.12), the merged result is the MLS water vapor anomalies minus the difference between mean MLS water vapor anomalies (blue dashed line) and mean merged result (black dashed line), both averaged during the overlap period.

An comparison between our merged data and two other merged satellite datasets, Stratospheric Water and OzOne Satellite Homogenized (SWOOSH) (S. Davis et al., 2016) and Global OZone Chemistry And Related trace gas Data records for the Stratosphere (GOZCARDS) (Froidevaux et al., 2015), shown in Figure S1, reveals good agreement among these datasets, with the exception of SWOOSH at 1 hPa after about 2003. The reason for this difference is not known.

### 2.3. SD-WACCM

CEMS2 (WACCM6) is the whole atmosphere component of the Community Earth System Model, v2 (CESM2), with fully coupled chemistry (see Gettelman et al., 2019, for a full description). It covers the range of altitude from the Earth's surface to the lower thermosphere (~140 km). In this paper, we use a specified dynamics (SD) version of WACCM6, where the temperature, horizontal winds, and vertical velocity below 50 km are nudged to MERRA2 (Molod et al., 2015) reanalysis data. The horizontal resolution is 0.95° latitude × 1.25° longitude, and the model uses a finite volume dynamical core (Lin, 2004). There are 88 vertical levels in SD-WACCM nudged by MERRA2, with 72 MERRA2-levels from the surface to the lower mesosphere and 16 free-running levels above (N. Davis et al., 2020). We emphasize that in the SD-WACCM simulation water vapor is calculated explicitly in the model, not nudged from MERRA2.

Our study is based on SD-WACCM because the specified dynamics run follows the temperature field and circulation in MERRA2, which is important for comparing the model to observations. Previous studies have shown that an earlier, free-running version of WACCM, CESM1(WACCM4) (Marsh et al., 2013), produces too small a trend of water vapor in the past 2 decades compared to observations, but the specified dynamics version of that model shows better agreement (Froidevaux et al., 2019; Yue et al., 2019). We first validate the SD-WACCM6 water vapor trend with our merged satellite data, and then analyze the water vapor variation in SD-WACCM6 model output. Our SD-WACCM run covers the period 1975–2019. MERRA2 data is available from 1980. To allow the age-of air tracer and longer-lived chemical species in the model to reach equilibrium, the SD-WACCM run starts from 1975 and nudges 1975–1979 fields with 1980–1984 MERRA2 data. We analyze the monthly mean model output from 1980 to 2019.

# 2.4. Validation of SD-WACCM6 Water Vapor Trend With Satellite Data

Our calculation of the water vapor trend follows a multi-variate linear regression (MLR) strategy similar to that used by Yue et al. (2015); Yue et al. (2019). The regression model is given by:

$$H_2O_{fit} = a \cdot QBO1 + b \cdot QBO2 + c \cdot ENSO + d \cdot F10.7 \tag{1}$$

The contributions of the QBO, ENSO, and the 11-year solar cycle to temperature variability are estimated by MLR, Equation 1, and the trend is then calculated from simple linear regression of the "filtered" time series:

$$H_2O_{filtered} = H_2O - H_2O_{fit} = A \cdot t + r \tag{2}$$

where A is the trend. In Equation 1, we use the NINO3.4 index as an indicator of the ENSO signal (https://www.ncdc.noaa.gov/teleconnections/enso/indicators/sst/); the 30 hPa and 50 hPa equatorial zonal-mean zonal wind as two independent indicators of the QBO (https://psl.noaa.gov/data/correlation/qbo.data); and the 10.7 cm radio flux as an indicator of the solar cycle (https://lasp.colorado.edu/lisird/data/noaa\_radio\_flux/). We also calculate the 2-sigma uncertainty range of the trend, with auto-correlation considered (Tiao et al., 1990).

An improvement to Yue et al.'s approach is that, when we regress on ENSO, we use the NINO3.4 index time series lagged by 5 months, since this lag time has the largest correlation with water vapor entering the middle atmosphere (Calvo et al., 2010; Garcia et al., 2007). When regressing on ENSO at higher altitudes, we lag the ENSO index by 5 months plus the age of air (AOA) difference between the tropical tropopause and each pressure level. The AOA is calculated using a synthetic, inert, linearly increasing AOA tracer in SD-WACCM.

YU ET AL. 5 of 18



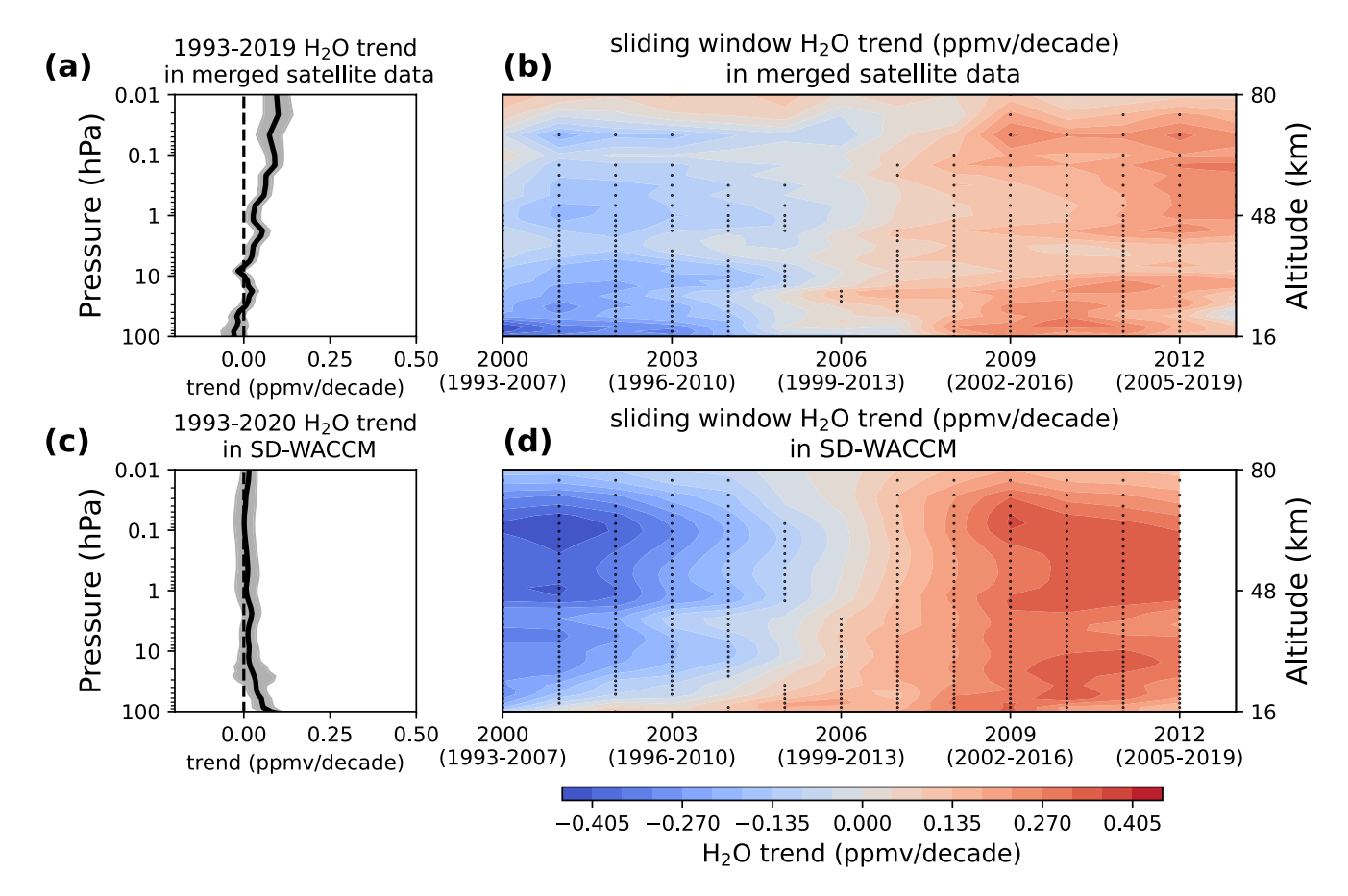


Figure 2. (a) Vertical profile of the mean water vapor mixing ratio trend averaged over 30°N–30°S for the period 1993–2020 in the merged satellite data. The dark shading denotes the 2-sigma uncertainty range. (b) The time series of 15-year sliding trends of 30°N–30°S mean water vapor from 100 hPa to 0.01 hPa, calculated using model output from 1980 to 2019 (the first 15-year trend is over 1993–2007 and centered on 2000) in our merged data. Dark gray dots denote where the trend exceeds the 2-sigma uncertainty range. (c and d) Same as in (a and b) but calculated from specified-dynamics version of the Whole Atmosphere Community Climate Model (SD-WACCM) output.

The trend of middle atmospheric water vapor is close to zero over 1993–2020, in both satellite observations and SD-WACCM (Figures 2a and 2c). In the stratosphere, both the satellite data and SD-WACCM show no significant trend of water vapor. In the mesosphere, the merged satellite data shows a small but significant trend, which is not reproduced in SD-WACCM. We do not see the positive trend observed in the Boulder frost point hygrometer (Hurst et al., 2011; Lossow et al., 2018). Although our analysis is mainly focused on the tropics (and thus not directly comparable to the Boulder hygrometer observations), previous studies that extend their analyses to northern hemisphere mid-latitudes also see this difference; the difference has been attributed mainly to the fact that the FPH observes a lower water vapor content than the satellite before 2000 (S. Davis et al., 2016; Hegglin et al., 2014). It has been pointed out by Hurst et al. (2016) that the discrepancy between the FPH and MLS could be a result of the slow drifting problem of MLS (Livesey et al., 2021). However, as we show in Figure 1, the variation of MLS v5.0 water vapor, where the slow drifting problem is partially resolved (Livesey et al., 2020), is consistent with that in SABER, and SABER water vapor does not have a slow drifting problem. Thus, our conclusion that there is no trend of water vapor in the past three decades is reasonable.

To further validate the SD-WACCM model output with the satellite observations, we show the 15-year sliding window trend of water vapor from 1993 to 2019 (2020 for the merged satellite data) in Figures 2b and 2d. We calculate the sliding window trends from the H<sub>2</sub>O time series obtained after removing contributions from ENSO, QBO, and the solar cycle over 1993–2019, per Equations 1 and 2. This obviates inaccuracies that might arise when attempting to remove the 11-year solar signal from the relatively short 15-year segments used to calculate sliding trends. Overall, the SD-WACCM middle atmospheric variation shows good agreement with satellite observations. One evident area of agreement is that both the model and observations show a negative trend pattern

YU ET AL. 6 of 18



before 2005 (the sliding window over 1998–2012), and a positive trend pattern thereafter; the SD-WACCM trend is larger over both the negative and positive trend eras by  $\sim$ 0.05 ppmv/decade; the overestimate of the observed trend by SD-WACCM is most pronounced in the mesosphere. Despite this difference, the overall consistency between satellite data and SD-WACCM lends confidence to the analysis of the water vapor trend based upon the model. In the following sections, our analyses are all based on SD-WACCM.

# 3. Drivers of Upper Stratospheric and Mesospheric Changes in SD-WACCM

The sources of water vapor in the middle atmosphere are direct entry from the troposphere at the tropical tropopause, and methane oxidation in the upper stratosphere and the mesosphere. The main sink is the photodissociation at wavelengths near Lyman-alpha in the mesosphere. As explained in Section 2.4, when we calculate the trend, we regress out the influence of solar activity, which strongly modulates the sink of water vapor above the upper mesosphere. Thus, the trend we estimate is only related to the variation of water vapor sources. Furthermore, in this paper we only analyze the changes of the sources of water vapor up to 0.1 hPa, avoiding most of the altitude range where photolytic loss is important.

In the upper stratosphere and mesosphere, we separate water vapor into water vapor from methane oxidation  $(H_2O_{fromCH4})$  and water vapor from direct entry into the stratosphere  $(H_2O_{entry})$  and quantify their respective contributions to the total water vapor trend. The accurate determination of  $H_2O_{fromCH4}$ , or how much methane is oxidized into water vapor, depends on several factors, such as how much methane enters the stratosphere, and the residual circulation that transports methane through the middle atmosphere. Figure 3a shows the time series of methane entering the stratosphere  $(CH_{4entry})$  calculated in SD-WACCM and averaged over  $10^{\circ}S-10^{\circ}N$  at 85 hPa. We note that the lower boundary condition on methane in SD-WACCM is based on observations, as described by Meinshausen et al. (2017) and that the time series at the tropical tropopause follows closely the boundary condition, since methane is well mixed throughout the troposphere.  $CH_{4entry}$  shows an overall increasing trend from  $\sim 1.5$  ppmv to  $\sim 1.9$  ppmv from 1980 to 2019, an increase of 27%. The increasing trend is rapid over 1980–1994 (0.09 ppmv per decade), becomes considerably slower over 1995–2012 (0.04 ppmv per decade), and is rapid again after 2013 (0.13 ppmv per decade).

The mean AOA reflects the strength of the residual circulation (Hall & Plumb, 1994). Our calculation of the AOA is based on the AOA tracer in SD-WACCM. This tracer is inert and increases linearly with time. We use the 85 hPa 10°S–10°N mean AOA tracer mixing ratio as a reference value, and use the time lag technique to calculate the AOA (Garcia et al., 2007). The AOA calculation in SD-WACCM is largely dependent on the MERRA2 wind field it nudges to. Previous studies have compared the AOA derived from several reanalysis data and concluded that the mean age of MERRA2 is similar to that from ERA5, and is longer than from ERA-interim and JRA-55 (Ploeger et al., 2019, 2021).

The overall AOA decreases over the past four decades. Take 10 hPa as an example (Figure 3b): at that level, AOA decreases from about 3.5 to 3.0 years over 1980–2019, with fluctuations to values as low as 2.6 years, such that the time-mean age on 10 hPa is ~3 years. The AOA changes are not uniform: AOA decreases by 0.11 years per decade from 1980 to June 2002, and then increases by 0.12 years per decade from July 2002 through 2019. The variability of the AOA is an indicator of the changes of the Brewer-Dobson circulation. More details on the Brewer-Dobson circulation and possible causes for its variability will be discussed in Section 5.

With the foregoing in mind, we calculate water vapor derived from methane oxidation,  $H_2O_{fromCH4}$ , based on the assumption:

$$H_2O_{fromCH4}(t, z, \theta) = 2 \times CH_{4oxidized}(t, z, \theta) = 2 \times (CH_4(t_0, z_0, \theta_0) - CH_4(t, z, \theta))$$
(3)

where  $\theta$  is latitude and z is log-pressure altitude;  $\theta_0$  and  $z_0$  denote the reference position at the tropical tropopause, that is,  $10^{\circ}\text{N}-10^{\circ}\text{S}$  and 100 hPa; and t0 is the time when an air parcel is on the reference position. The mean AOA  $\tau = t - t_0$  is the difference between the time, t, when a certain mixing ratio of the AOA tracer is found at a particular point  $(z, \theta)$  in the meridional plane, and the (earlier) time when the same mixing ratio occurred at the reference point  $(z_0, \theta_0)$ . Similar methods can be found in Austin et al. (2007) and Oman et al. (2008). Some previous studies conclude that molecular hydrogen also plays a role in middle atmospheric water vapor budget, especially in upper stratosphere (le Texier et al., 1988; Wrotny et al., 2010). However, in SD-WACCM model, the

YU ET AL. 7 of 18



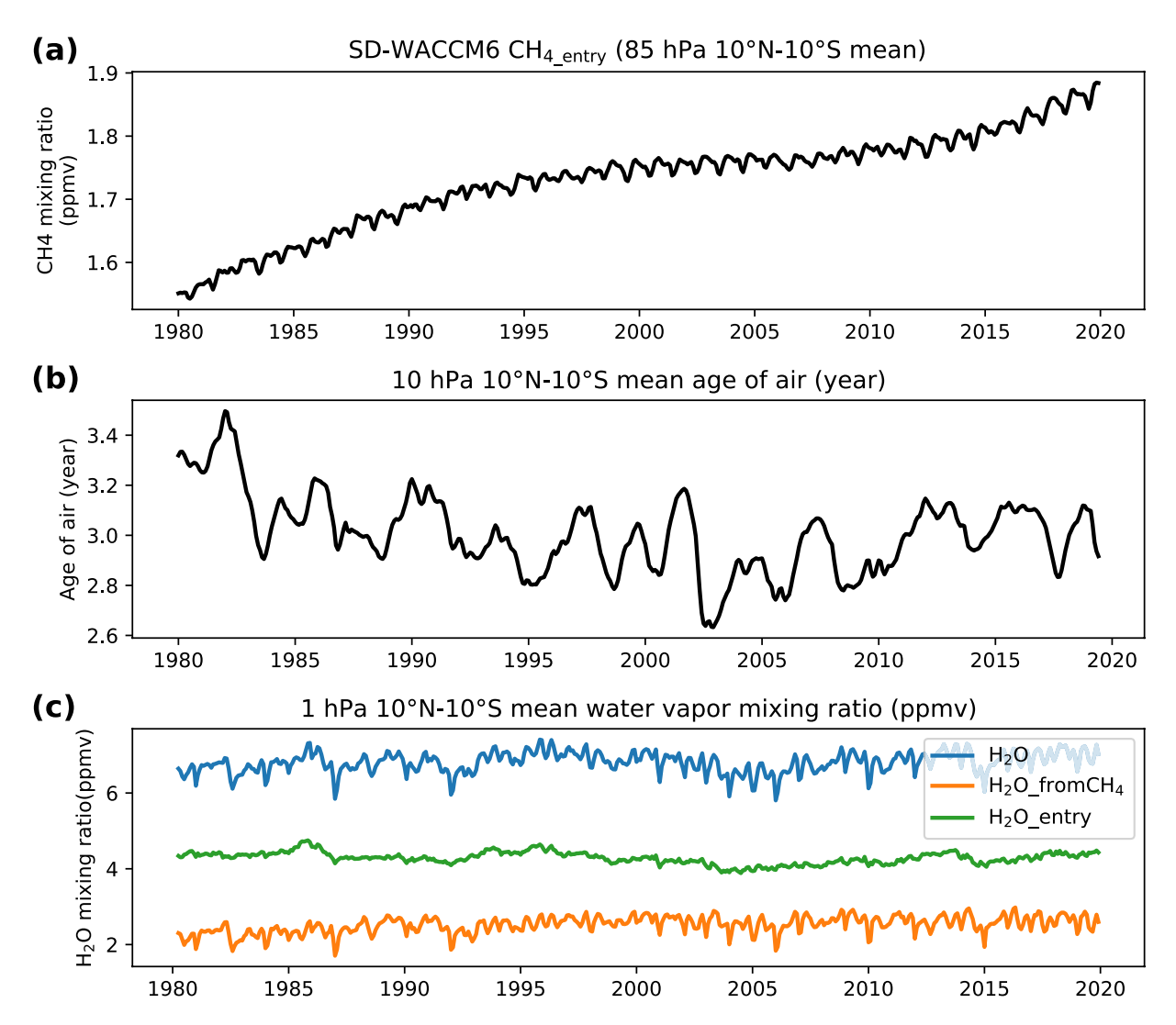


Figure 3. (a) Time series of  $CH_{4\text{entry}}$  at 85 hPa, averaged over  $10^\circ N - 10^\circ S$ . (b) Time series for mean age of air (years) at 10 hPa, averaged over  $10^\circ N - 10^\circ S$ . (c) Time series of  $H_2O$  (blue line),  $H_2O_{\text{from}CH4}$  (orange line), and  $H_2O_{\text{entry}}$  (green line) at 1 hPa, averaged over  $10^\circ N - 10^\circ S$ .

variation of  $H_2$  with altitude in the stratosphere is less than 0.1 ppmv and its role in the decadal variation is even smaller, so we neglect this process.

We calculate  $H_2O_{entry}$  as follows: in the stratosphere and lower mesosphere,  $H_2O_{entry}$  equals SD-WACCM water vapor mixing ratio minus  $H_2O_{fromCH4}$  calculated from Equation 3. However, in the middle and upper mesosphere, above about 0.3 hPa (~57 km), water vapor and methane begin to be photodissociated (Brasseur & Solomon, 1984), such that the sum of total molecular hydrogen,  $H_2O + 2CH_4$ , is no longer constant. Therefore, the simple subtraction of (3) from the total water vapor is no longer appropriate for estimating how much water vapor is due to  $H_2O_{entry}$ . Instead, above 0.3 hPa we limit the proportions of  $H_2O_{fromCH4}$  and  $H_2O_{entry}$  relative to total water vapor to their values at 0.3 hPa; we also reduce  $H_2O_{entry}$  and  $H_2O_{fromCH4}$  above 0.3 hPa in proportion to the reduction of total water vapor above that pressure level, such that the sum  $H_2O_{entry} + H_2O_{fromCH4}$  remains equal to total water vapor everywhere. We have compared  $H_2O_{entry}$  from the time series of water vapor mixing ratio at the entry point extended to higher altitudes by taking into account the time required to reach those altitudes (i.e., the AOA), and find that the difference between the two values, anywhere between 100 hPa and 0.01 hPa, is at most 0.37 ppmv and, on average, 0.17 ppmv.

While our partitioning of total water into  $H_2O_{entry}$  and  $H_2O_{fromCH4}$  cannot account for methane oxidation above 0.3 hPa, this does not introduce much error because the amount of unoxidized methane in the upper mesosphere

YU ET AL. 8 of 18



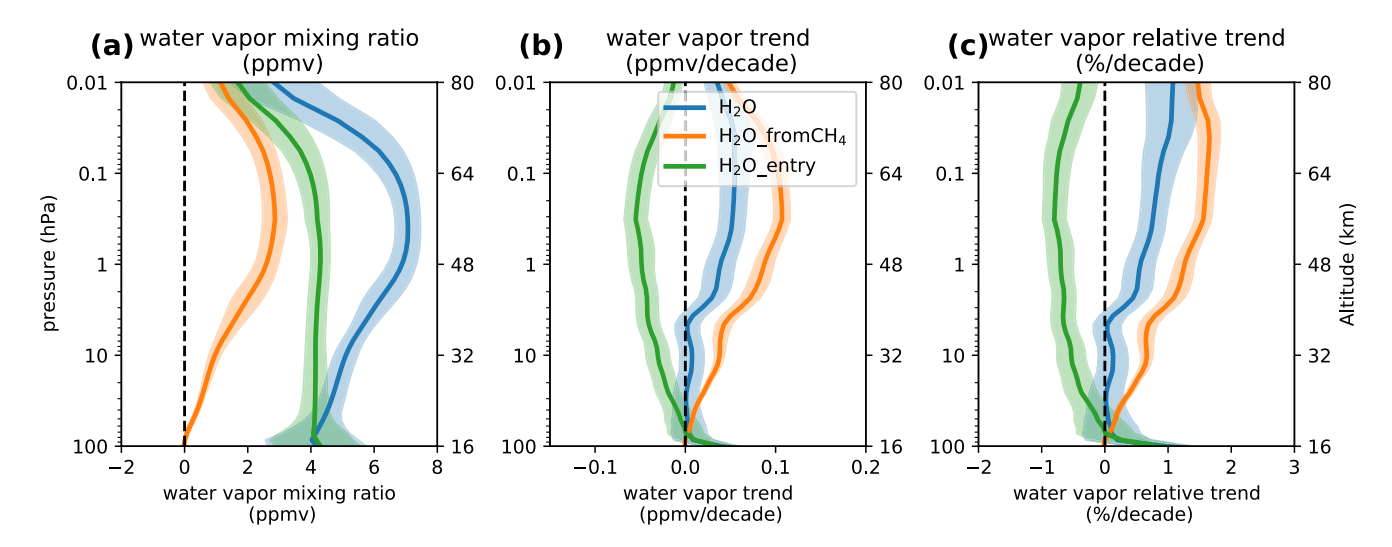


Figure 4. (a) The 1980–2019,  $30^{\circ}$ N– $30^{\circ}$ S mean water vapor mixing ratio in specified-dynamics version of the Whole Atmosphere Community Climate Model (blue line), and the partitioning into  $H_2O_{fromCH4}$  (orange line) and  $H_2O_{entry}$  (green line). (b) Same as in (a), but for the trend (ppmv per decade). (c) Same as in (a), but for the relative trend (% per decade). The shading denotes the 2-sigma uncertainty range.

is small, about 10%–15% of its value at the tropopause. In addition, at these altitudes, photodissociation instead of oxidation becomes the dominant loss process for methane, such that loss of methane does not imply production of water vapor. Thus, above 0.3 hPa, any additional contribution to water vapor from methane is small and negligible. Note also that our approximation does not introduce much error for the purpose of computing trends. The water vapor variability due to photodissociation is mainly influenced by changing solar activity associated with the 11-year solar cycle, which we filtered out using multi-variate regression before calculating the trend. Thus, most of the contribution of photodissociation to water vapor trends above 0.3 hPa is removed in this study.

We focus on the stratopause (1 hPa) as an example of how partitioning total water vapor into  $H_2O_{entry}$  and  $H_2O_{fromCH4}$  works. The water vapor mixing ratio on this level is ~6.8 ppmv (see Figure 3c).  $H_2O_{fromCH4}$  is ~2.6 ppmv and accounts for 38.2% of the water vapor at the stratopause, while  $H_2O_{entry}$  is ~4.2 ppmv and accounts for 61.8% of the water vapor at the stratopause. In terms of the vertical profile (Figure 4a),  $H_2O_{fromCH4}$  increases from 0 to 2.9 ppmv between the tropical tropopause and the middle mesosphere, and the pressure levels where  $H_2O_{fromCH4}$  increases most rapidly with altitude are between 10 hPa and 1 hPa (Figure 4a).  $H_2O_{entry}$  shows a constant value of 4 ppmv in both stratosphere and mesosphere below 0.3 hPa, before photodissociation becomes important. These values agree with previous observations and model simulations (e.g., Rosenlof, 2002). Thus, separating  $H_2O_{fromCH4}$  and  $H_2O_{entry}$  based on the AOA is feasible.

Over 1980–2019, water vapor in SD-WACCM has almost no trend in the lower and middle stratosphere but has a positive trend of up to 0.07 ppmv per decade above the middle stratosphere, where methane oxidation is rapid (Figure 4b). Due to the increase of methane oxidation with altitude, the trend of  $H_2O_{fromCH4}$  increases to 0.09 ppmv per decade around the middle stratosphere, and to 0.13 ppmv per decade in the upper stratosphere and mesosphere. On the other hand,  $H_2O_{entry}$  shows a negative trend of -0.05 ppmv per decade throughout most of the altitude range, except near 100 hPa, where the trend is actually positive. This discrepancy is due to the lag between the time air parcels enter the stratosphere at 100 hPa and the time they reach higher levels. For example, it takes 3 years for air to travel from the entry point to 10 hPa (Figure 3a), so the trend of  $H_2O_{entry}$  on 10 hPa is the trend of the entry values a few years earlier, 1977–2016 instead of 1980–2019. At levels above 50 hPa, the negative trend of  $H_2O_{entry}$  is offset by the positive water vapor trend from methane oxidation,  $H_2O_{fromCH4}$ ; thus, the total water vapor increase is negligible over 1980–2020 through the middle stratosphere and small but positive in the upper stratosphere and mesosphere.

To understand the reasons for the variation of water vapor trend on decadal scales, we show 15-year sliding trends of  $H_2O$ ,  $H_2O_{fromCH4}$ , and  $H_2O_{entry}$  in Figure 5. These plots are similar to those shown in Figure 2, but in this case cover the entire period of the SD-WACCM simulation and, in addition, they show the behavior partitioned according to the water vapor source. SD-WACCM correctly reproduces the three different eras of water vapor

YU ET AL. 9 of 18



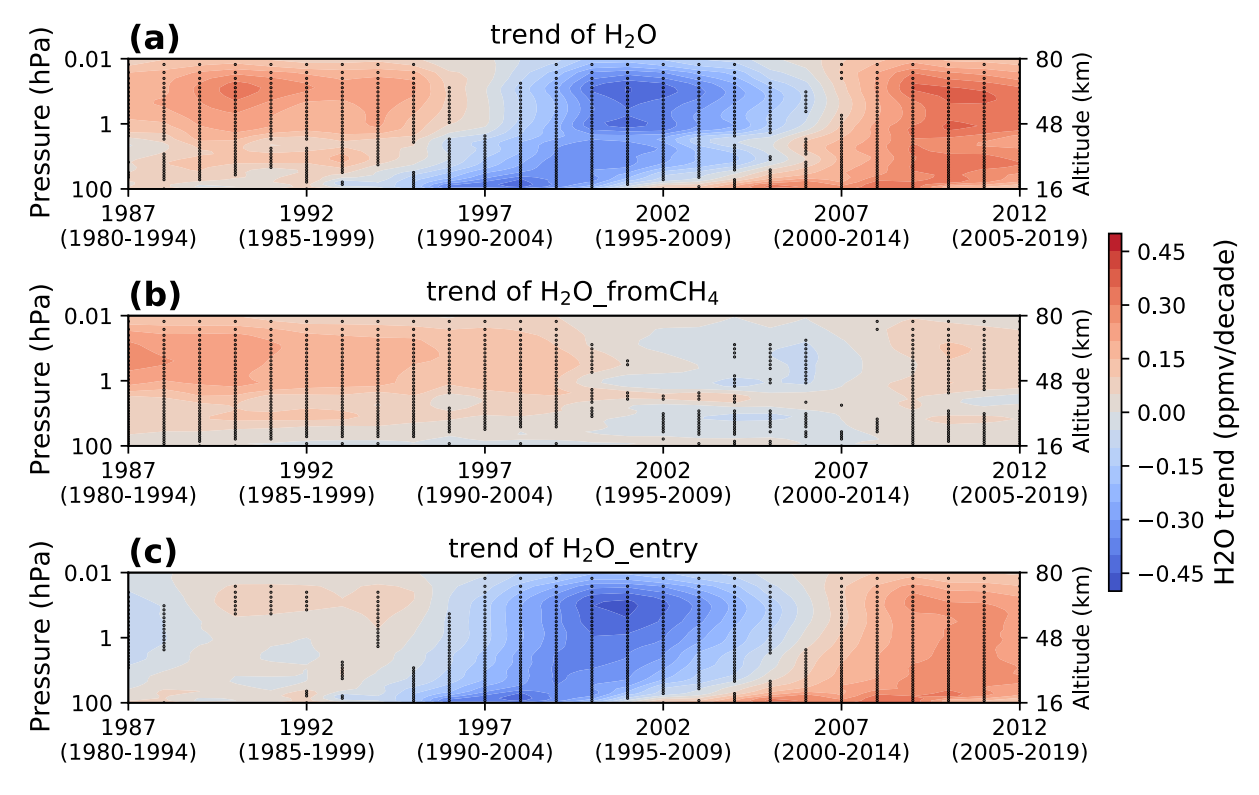


Figure 5. (a). The time series of 15-year sliding trends of  $30^{\circ}N-30^{\circ}S$  mean water vapor from 100 hPa to 0.01 hPa, calculated using SD-WACCM6 model output from 1980 to 2019 (the first 15-year trend is centered on 1986 and the last on 2012). Black dots denote where the trend is exceeds the 2-sigma uncertainty range. The total trend (a) then is divided into (b and c), where (b) is the trend of  $H_2O_{from CH4}$  and (c) is the trend of  $H_2O_{entro}$ . See text for details.

trend as observed with the merged data after 1993 (cf. Figure 2), and previous other studies: water vapor increases by up to 0.30 ppmv per decade over 1980–1998, decreases by up to 0.37 ppmv per decade over 1998–2003, and then increases by up to 0.33 ppmv per decade after 2003.

Methane oxidation and water vapor entering the middle atmosphere from the troposphere play different roles over these three eras. Before  $\sim$ 1995, the positive trend of water vapor is mainly driven by the increase of  $H_2O_{fromCH4}$  (Figure 5b), and the trend of  $H_2O_{entry}$  is insignificant (Figure 5c). After 1995, the increase of  $H_2O_{fromCH4}$  becomes slower, and both the large drop of middle atmospheric water vapor over 1998–2003 and the increase after 2003, are mainly driven by the changes of  $H_2O_{entry}$ .

As mentioned earlier in this section, the methane emission rate also could be divided into three eras: rapid (1980–1994) – slow (1995–2012) – rapid (after 2013).  $H_2O_{fromCH4}$  does not recover to a high positive trend immediately after 2013, since it takes several years for methane to be transported to the upper stratosphere and mesosphere and our record ends in 2019. We would expect that, in later years, methane oxidation will again become a significant driver to a future increase of water vapor content in the upper stratosphere and mesosphere.

# 4. Trends in the Lower Stratosphere: The Role of Cold Point Temperature in H<sub>2</sub>O<sub>entry</sub>

As shown above,  $H_2O_{entry}$  explains most of the changes of the middle atmospheric water vapor after 1995, including the large drop over 1998–2003 and then the increase after 2003. In this section, we focus on the tropical lower stratosphere, and quantify the changes of  $H_2O_{entry}$ . The cold point temperature ( $T_{CP}$ ) plays the most important role in determining  $H_2O_{entry}$  (e.g., Fueglistaler & Haynes, 2005; Mote et al., 1996; Randel et al., 2004), and deep convection and the overshooting events that penetrate the tropopause may determine the rest. In this section, our strategy is to separate the part of water vapor variation that could be explained by the cold point temperature ( $H_2O_{temp}$ ), and check (a) whether the residual ( $H_2O_{residual}$ ) contributes to the decadal variation of the water vapor, and (b) how  $H_2O_{residual}$  is connected with deep convection.

YU ET AL. 10 of 18



At the tropical tropopause, the regions with strong upwelling always have extremely low temperatures, and the low temperatures reduce the saturation mixing ratio and constrain the water vapor content entering the stratosphere. The regions with downwelling have higher temperatures but do not influence the water vapor entering the stratosphere. Thus, when calculating  $T_{\rm CP}$ , we average the temperature over 25°N–25°S using only the grid points where the vertical velocity in pressure coordinates is negative, that is, where the air ascends.

The cold point tropopause is located at 100 hPa during boreal summer and at 85 hPa during boreal winter (Oman et al., 2008). We consider the variation of the tropopause height by using a cubic spline interpolation method for the cold point tropopause between 118 hPa and 72 hPa and then picking up the minimum value on a grid with 1 hPa resolution. To account for different lag times for air parcels to travel from the cold point tropopause during different months, we use a similar method as in Randel and Park (2019). For water vapor data at each latitude, level, and month (Jan to Dec), we lag the time series of cold point temperature by 0–11 months with respect to the time series of water vapor and pick the lag month that maximizes the lagged correlation coefficient between water vapor and cold point temperature. For example, during May each year, the water vapor time series at 85 hPa and 5°N has the maximum correlation with the time series of  $T_{\rm CP}$  during April, so we use this as the predictor  $T_{\rm CP}$ . Then, for each latitude and level, we put together the corresponding  $T_{\rm CP}$  for all months, and regress on it the corresponding water vapor time series. Finally, we generate a 3-D (month-level-latitude) matrix of  $H_2O_{\rm temp}$ , and a 3-D matrix of  $H_2O_{\rm residual}$ .

The  $H_2O_{temp}$  we reconstruct has a is similar to the result of Randel and Park (2019); the correlation coefficient with is  $H_2O_{entry}$  on 85 hPa, averaged over 30°N–30°S (Figure 6a), is as high as 0.874. Not surprisingly, both the large negative trend of  $H_2O_{entry}$  over 1998–2003 and the positive trend after 2004 are explained by changes in the cold point temperature (Figures 6c and 6d).

Since most of the variation of  $H_2O_{entry}$  can be explained by the cold point temperature,  $H_2O_{residual}$  has a relatively small value (Figure 6b), and insignificant trend. We are also interested in how much deep convection might explain the variation of  $H_2O_{residual}$ . In the model's parameterization of deep convection, the highest level that the convective mass flux reaches is 139 hPa, which is below the cold point tropopause. Although there is no direct transport of water vapor from deep convection, the latter could still influence  $H_2O_{entry}$  by, for example, upper tropospheric mixing. We find that, at least in this version of SD-WACCM, there is no evidence that deep convection matters, since the value of the  $H_2O_{residual}$  and its trend are both relatively small, and they are not significantly correlated with deep convection (Figure 6b). The  $H_2O_{residual}$  could be influence by other factors, such as horizontal mixing (Ploeger et al., 2013; Ray et al., 2010),but we do not investigate this possibility in the specified dynamics simulations used here.

Although the convective parameterization in SD-WACCM may preclude a role for deep convection in the trend of middle atmospheric water vapor because it does not allow for overshooting events, model water vapor shows good agreement with observations. In other words, in the model, deep convection is not a key factor for the trend of water vapor in the past four decades. Dessler et al. (2016) argue that the deep convection may explain 0.2–0.5 ppmv of the increase of water vapor in the 21st century. Our result, which focuses mainly on the past, does not refute the possibility of future importance.

# 5. Discussion

In previous sections, we concluded that rapidly increasing anthropogenic methane emissions explain most of the increase of water vapor in the middle atmosphere before 1995. We also showed that the changes of the cold point temperature explain most of the variations of middle atmospheric water vapor after 1995 and we provide a thorough discussion on quantifying the role of methane and cold point temperature in the decadal-scale variability, and focus on the impact of each contribution. Our conclusions are consistent with previous studies; for example, Hurst et al. (2011) also points out the importance of methane oxidation, and Randel and Park (2019) also emphasize the importance of the cold point temperature.

In this section, we put our study into the larger context of climate change, discuss what might have influenced the cold point temperature in the past four decades, and attempt to connect it with anthropogenic activities.

We examined the relationship between the cold point temperature,  $T_{\rm CP}$ , and the transformed Eulerian mean (TEM) vertical velocity  $w^*$  as follows: After deseasonalizing both time series, we used multi-variate linear regression

YU ET AL. 11 of 18



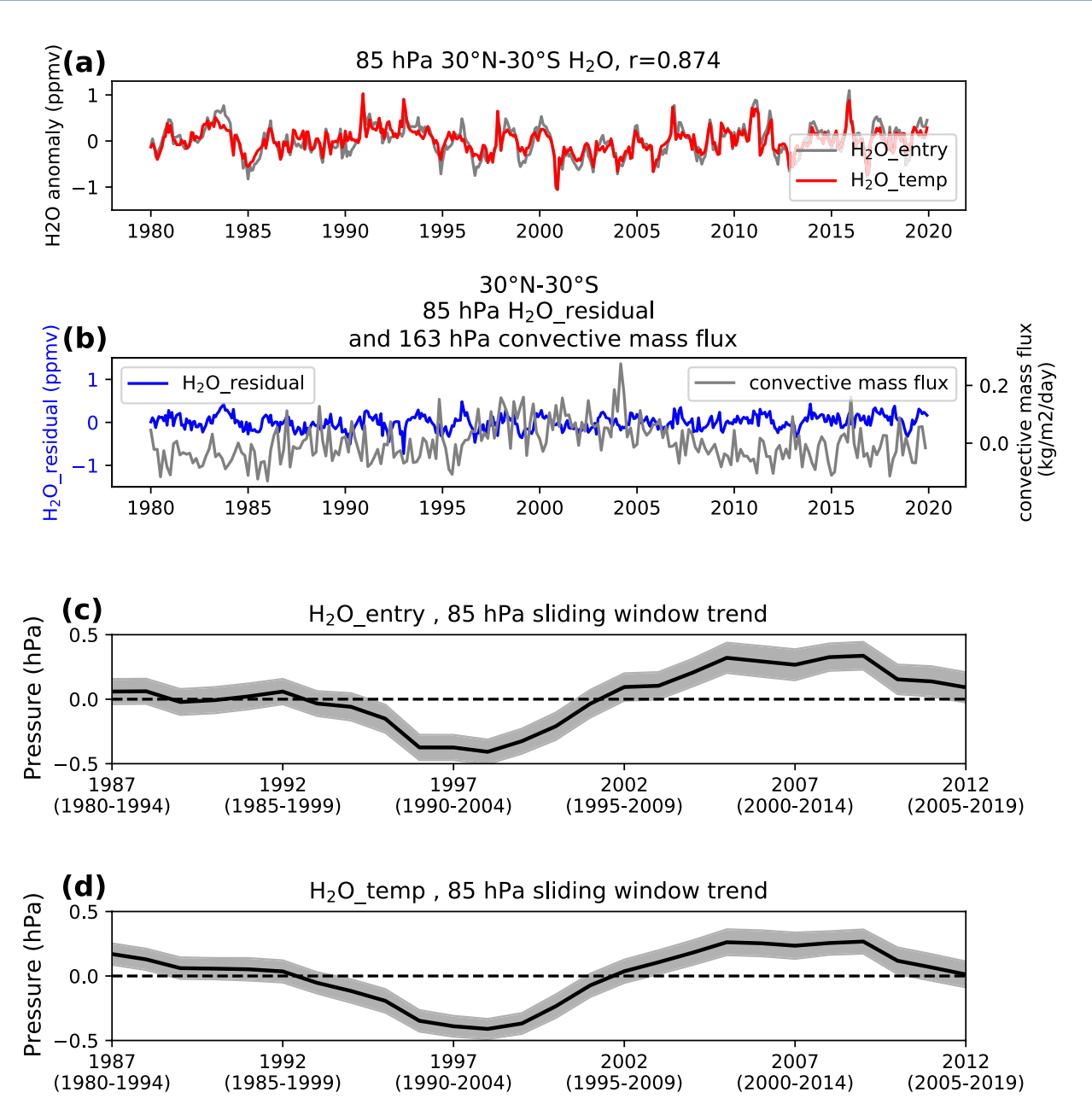


Figure 6. (a) Time series of deseasonalized  $H_2O_{entry}$  (gray line) and  $H_2O_{temp}$  (red) at 85 hPa, averaged over 30°N-30°S; the correlation coefficient is 0.874. (b) Time series of deseasonalized  $H_2O_{residual}$  at 85 hPa, averaged over 30°N-30°S (blue), and time series of the deseasonalized convective mass flux at 163 hPa, averaged over 30°N-30°S. (c) The time series of 15-year sliding trend of mean  $H_2O_{entry}$  at 85 hPa, 30°N-30°S, calculated from 1980 to 2019. Gray shading denotes the 2-sigma uncertainty range. (d) Same as in (c), but for the trend of  $H_2O_{temp}$ . See text for details.

to remove the signals of the QBO, ENSO, and volcanic eruptions to avoid any correlation caused by the fact that both time series could be influenced by these factors. We then regressed  $T_{\rm CP}$  on  $w^*$  and found a correlation coefficient of -0.59 (Figure 7). This result suggests that  $w^*$  influences the variation of the cold point temperature on both monthly and decadal scales; it shows a decreasing trend before 2003 and an increasing trend thereafter, consistent with the decadal variation of the cold point temperature.

A causal relationship between the Brewer-Dobson circulation and the cold point temperature could be supported by the simplified TEM thermodynamic equation (Andrews et al., 1987):

$$\frac{dT}{dt} = -w^*S + Q_{net} \tag{4}$$

YU ET AL. 12 of 18



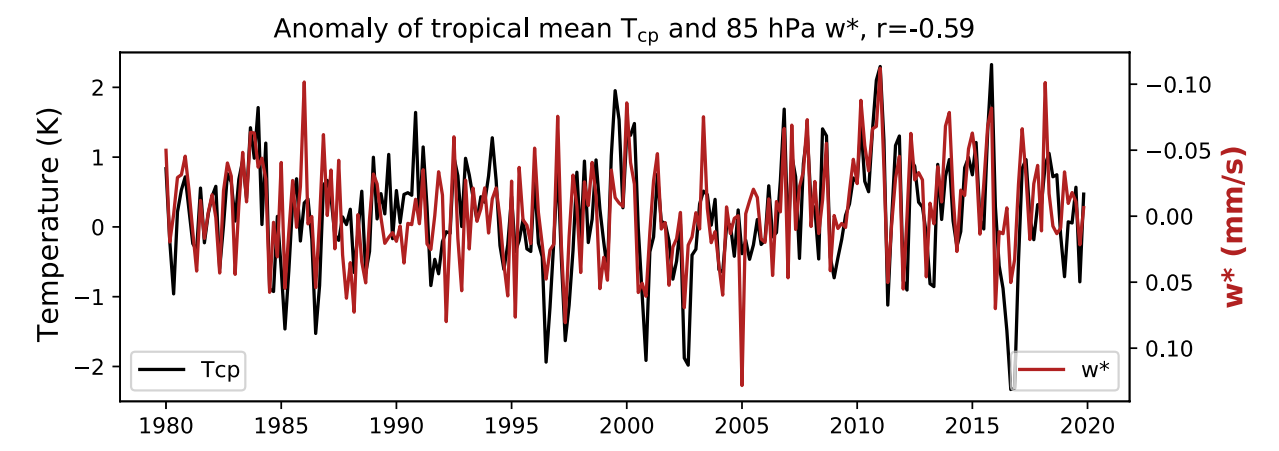


**Figure 7.** The time series of the tropical mean cold point temperature anomaly in specified-dynamics version of the Whole Atmosphere Community Climate Model (black line) and 85 hPa tropical mean  $w^*$  (transformed Eulerian mean residual circulation vertical velocity, red line); in both cases, the signal of El Niño-Southern Oscillation, quasi-biennial oscillation, and volcanic eruptions is removed.

where horizontal mean advection, eddy flux divergences and diffusion have been neglected. In Equation 4,  $w^*$  is the TEM residual circulation vertical velocity, S is the static stability, and  $Q_{\text{net}}$  is the net heating rate (longwave + shortwave heating rate). The largest contribution to dT/dt is the seasonal cycle, which has been removed in our analysis. Taking this into account and expressing  $Q_{\text{net}}$  as radiative relaxation, Equation 4 can be rewritten as:

$$w^*S = -\alpha T \tag{5}$$

where  $\alpha$  is an inverse radiative time scale. Thus, we conclude that, an increase of  $w^*$ , that is, an acceleration of the Brewer-Dobson circulation can lead to a decrease of the cold point temperature, and vice-versa.

One possible explanation for the variation of the Brewer-Dobson circulation is anthropogenic activity, especially ozone depletion and recovery. Many studies have noted the impact of anthropogenic activity on the Brewer-Dobson circulation and the cold point temperature. Greenhouse gases can influence the Brewer-Dobson circulation either by changing the sea surface temperature or by directly changing the radiative budget, and a monotonically increasing trend in greenhouse gases leads to an acceleration of the Brewer-Dobson circulation (Garcia & Randel, 2008; Li et al., 2018; Maycock et al., 2013; Morgenstern et al., 2018; Oberländer-Hayn et al., 2015; Oman et al., 2008). An interesting factor is the depletion and recovery of ozone, which is not monotonic. After ozone depleting substances reached their peak abundances at about 2000, they began to decrease because of the success of the Montreal protocol (Newman et al., 2007), and the ozone hole over Antarctica began to recover (Solomon et al., 2016). Ozone depletion alone can cause acceleration of the Brewer-Dobson circulation, and its recovery can cause deceleration of the Brewer-Dobson circulation, and its recovery can cause deceleration of the Brewer-Dobson circulation (Fu et al., 2019; Li et al., 2018; Polvani et al., 2018, 2019).

One should note that, although plausible, the causal relationship between ozone depletion/recovery and the variation of the Brewer-Dobson circulation is not statistically significant in our study. On the one hand, changes of ozone influence  $w^*$  most strongly in the Southern Hemisphere (Fu et al., 2019; Polvani et al., 2018), while our study mainly focuses on the Tropics. On the other hand, Polvani et al. (2018); Polvani et al. (2019) concluded that the tropical Brewer-Dobson circulation will still accelerate over the 21st century due to the influence of both ozone recovery and greenhouse gas emissions, but the acceleration is much slower than during the period of ozone loss, 1960–2000. Note that the Polvani et al. (2018) conclusion about the acceleration of the circulation in the 21st century is based on the trend calculated over 80 years; in our study, where we only have a two-decade record in the 21st century, we see a slight deceleration of the Brewer-Dobson circulation (Figures 3b and 7). Whether this is because our record is not long enough or there are other explanations for the variation of the Brewer-Dobson circulation is not clear.

Overall, we find that the variation of the Brewer-Dobson circulation influences substantially the variation of the cold point temperature, and thus  $H_2O_{entry}$ , on both monthly and decadal time scales. Our results also suggest that

YU ET AL. 13 of 18



the variation of the Brewer-Dobson may be influenced by anthropogenic activity, such as greenhouse gas emission and ozone depletion and recovery.

#### 6. Conclusions

According to Yue et al. (2019), the zonal and meridional averaged water vapor in the middle atmosphere over 55°N–55°S, as observed by both SABER and MLS, has increased 2%–5% per decade since the early 2000s. This is consistent with our findings using a merged HALOE-MLS-SABER data set and a simulation carried out with SD-WACCM in the tropics (Figure 5). On the other hand, water vapor in the stratosphere shows no significant trend over a longer period (the past three decades in either the merged satellite data or SD-WACCM, or the past four decades in the SD-WACCM simulation). The significant increasing trend over 1980–2020 observed by the FPH over Boulder is not reproduced. The FPH trend could be due to local variations not captured in satellite observations and global models. The merged satellite data indicate a 1%–2% per decade increase of mesospheric water vapor over 1993–2020, which is, however, not simulated by SD-WACCM. Except for this discrepancy, SD-WACCM simulates water vapor trends that agree closely with the observations, which suggests that the model can be used to analyze the processes that control water vapor trends.

In this paper, we separated SD-WACCM water vapor in the middle atmosphere into different sources, calculating their contribution to the overall trend, and analyzing how the contributions change over time based on SD-WACCM. In the upper stratosphere, we conclude that changes in water vapor derived from methane oxidation explain most of the increase of water vapor before 1995, and that changes in water vapor entering the stratosphere from the troposphere mainly explain the large drop between 1998 and 2003 and then the increase of water vapor after 2003.

In the lower stratosphere, we reconstructed water vapor based on the cold point temperature and considered the seasonal variability of the cold point tropopause. The water vapor reconstruction indicates that changes in cold point temperature explain most of the variation of water vapor entering the stratosphere. We then compared the residual water vapor (actual minus reconstructed) with deep convective mass flux in SD-WACCM, and found that the latter plays an insignificant role in past changes of water vapor in the middle atmosphere, at least in this model.

Changes of water vapor in the middle atmosphere are strongly connected with anthropogenic activities. Rapidly increasing anthropogenic methane emissions contribute to an increase of water vapor in the middle atmosphere, especially before 1995. Ozone depletion before 2000, and recovery after 2000, may in turn accelerate and decelerate the Brewer-Dobson circulation, which then leads to a decrease and then an increase in the cold point temperature and hence in water vapor.

The rate of emission of methane increases again after 2013, indicating that the contribution from methane oxidation to water vapor will increase in the future. Ozone will keep recovering until 2080 according to projections by multiple models (e.g., Polvani et al., 2019). The recovery of ozone may influence the Brewer-Dobson circulation, offsetting part of the acceleration due to increases in greenhouse gases such as  $CO_2$  over the period studied here. Together with future changes in the emission of methane, how these anthropogenic processes will combine and influence the future water vapor trend is unclear. The analysis presented in this paper will help quantify the contribution from methane, ozone, and greenhouse gases such as  $CO_2$  to the future budget and trends of middle atmospheric water vapor.

# **Data Availability Statement**

- [Dataset] SABER v2.07 water vapor data are available from http://saber.gats-inc.com/data.php (see Russell et al., 1999)
- [Dataset] MLS v5.0 water vapor data are available from https://disc.gsfc.nasa.gov/datasets/ML2H2O\_005/summary (see Waters et al., 2006)
- [Dataset] HALOE water vapor data are available from http://haloe.gats-inc.com/download/index.php (see Russell et al., 1993)
- [Dataset] SWOOSH data are available from https://csl.noaa.gov/groups/csl8/swoosh/ (see S. Davis et al., 2016)

YU ET AL. 14 of 18



- [Dataset] GOZCARDS data are available from https://earthdata.nasa.gov/esds/competitive-programs/measures/gozcards (see Froidevaux et al., 2015)
- [Software] CESM2-WACCM6 code are available from https://www.cesm.ucar.edu/models/cesm2/ (see Gettelman et al., 2019).
- [Dataset] The merged satellite data described in this paper are available from https://doi.org/10.5281/zenodo.6308969 (Yu et al., 2022a)
- [Software] All code associated with data analysis in this paper is available from https://doi.org/10.5281/zenodo.6774398 (Yu et al., 2022b)

#### Acknowledgments

All authors are supported by NASA's TIMED/SABER mission. WY, JY and JR are supported by NSF AGS1901126. RG is supported in part by NASA grant 80NSSC19K1214. We thank the SABER, MLS, and HALOE groups for providing the retrieved satellite data. We also thank Dr. Charles Bardeen for providing the SD-WACCM model output, and Drs. Ellis Remsberg, Bill Randel, Anne Smith, and Tao Wang for valuable discussions. We thank the constructive comments and suggestions made by three anonymous reviewers. The National Center for Atmospheric Research (NCAR) is sponsored by the U.S. National Science Foundation (NSF). WACCM is a component of the Community Earth System Model (CESM), which is supported by NSF and the Office of Science of the U.S. Department of Energy. Computing resources for the results presented here were provided by NCAR's Climate Simulation Laboratory, sponsored by NSF and other agencies, and enabled by the computational and storage resources of NCAR's Computational and Information Systems Laboratory (CISL).

# References

Andrews, D. G., Holton, J. R., & Leovy, C. B. (1987). Middle atmosphere dynamics (p. 40). Academic Press.

Austin, J., Wilson, J., Li, F., & Vömel, H. (2007). Evolution of water vapor concentrations and stratospheric age of air in coupled chemistry-climate model simulations. *Journal of the Atmospheric Sciences*, 64(3), 905–921. https://doi.org/10.1175/JAS3866.1

Bates, D. R., & Nicolet, M. (1950). The photochemistry of atmospheric water vapor. *Journal of Geophysical Research*, 55(3), 301–327. https://doi.org/10.1029/jz055i003p00301

Bonazzola, M., & Haynes, P. H. (2004). A trajectory-based study of the tropical tropopause region. *Journal of Geophysical Research*, 109(D20), D20112. https://doi.org/10.1029/2003jd004356

Brasseur, G., & Solomon, S. (1984). Aeronomy of the middle atmosphere: Chemistry and physics of the stratosphere and mesosphere. Springer. Brinkop, S., Dameris, M., Jöckel, P., Garny, H., Lossow, S., & Stiller, G. (2016). The millennium water vapour drop in chemistry-climate model simulations. Atmospheric Chemistry and Physics, 16(13), 8125–8140. https://doi.org/10.5194/ACP-16-8125-2016

Calvo, N., Garcia, R., Randel, W. J., & Marsh, D. R. (2010). Dynamical mechanism for the increase in tropical upwelling in the lowermost tropical stratosphere during warm ENSO events. *Journal of the Atmospheric Sciences*, 67(7), 2331–2340. https://doi.org/10.1175/2010JAS3433.1

Cooney, J. W., Bedka, K. M., Bowman, K. P., Khlopenkov, V. K., & Itterly, K. (2021). Comparing Tropopause-Penetrating Convection Identifications Derived From NEXRAD and GOES Over the Contiguous United States. *Journal of Geophysical Research: Atmospheres*, 126(14), e2020JD034319. https://doi.org/10.1029/2020JD034319

Davis, N., Davis, S. M., Portmann, R. W., Ray, E., Rosenlof, K. H., & Yu, P. (2020). A comprehensive assessment of tropical stratospheric upwelling in the specified dynamics Community Earth System Model 1.2.2—Whole atmosphere community climate model (CESM (WACCM)). Geoscientific Model Development, 13(2), 717–734. https://doi.org/10.5194/GMD-13-717-2020

Davis, S., Rosenlof, K. H., Hassler, B., Hurst, D. F., Read, W. G., Vömel, H., et al. (2016). The Stratospheric Water and Ozone Satellite Homogenized (SWOOSH) database: A long-term database for climate studies. *Earth System Science Data*, 8(2), 461–490. https://doi.org/10.5194/ESSD-8-461-2016

Dessler, A. E., Schoeberl, M. R., Wang, T., Davis, S. M., & Rosenlof, K. H. (2013). Stratospheric water vapor feedback. *Proceedings of the National Academy of Sciences of the United States of America*, 110(45), 18087–18091. (246pg Times Cited:82 Cited References Count:43). https://doi.org/10.1073/pnas.1310344110

Dessler, A. E., Schoeberl, M. R., Wang, T., Davis, S. M., Rosenlof, K. H., & Vernier, J. P. (2014). Variations of stratospheric water vapor over the past three decades. *Journal of Geophysical Research: Atmospheres*, 119(22), 12588–12598. https://doi.org/10.1002/2014JD021712

Dessler, A. E., Weinstock, E. M., Hintsa, E. J., Anderson, J. G., Webster, C. R., May, R. D., et al. (1994). An examination of the total hydrogen budget of the lower stratosphere. *Geophysical Research Letters*, 21(23), 2563–2566. https://doi.org/10.1029/94GL02283

Dessler, A. E., Ye, H., Wang, T., Schoeberl, M. R., Oman, L. D., Douglass, A. R., et al. (2016). Transport of ice into the stratosphere and the humidification of the stratosphere over the 21st century. *Geophysical Research Letters*, 43(5), 2323–2329. https://doi.org/10.1002/2016g1067991

Ding, Q., & Fu, Q. (2018). A warming tropical central Pacific dries the lower stratosphere. Climate Dynamics, 50(7–8), 2813–2827. https://doi.org/10.1007/s00382-017-3774-y

Dvortsov, V. L., & Solomon, S. (2001). Response of the stratospheric temperatures and ozone to past and future increases in stratospheric humidity. *Journal of Geophysical Research*, 106(D7), 7505–7514. https://doi.org/10.1029/2000jd900637

Evans, S. J., Toumi, R., Harries, J. E., Chipperfield, M. P., & Russell, J. M. (1998). Trends in stratospheric humidty and the sensitivity of ozone to these trends. *Journal of Geophysical Research*, 103(D8), 8715–8725. https://doi.org/10.1029/98JD00265

Fernando, A. M., Bernath, P. F., & Boone, C. D. (2020). Stratospheric and mesospheric H<sub>2</sub>O and CH<sub>4</sub> trends from the ACE satellite mission. Journal of Quantitative Spectroscopy and Radiative Transfer, 255, 107268. https://doi.org/10.1016/j.jqsrt.2020.107268

Flentje, H., Dörnbrack, A., Ehret, G., Fix, A., Kiemle, C., Poberaj, G., & Wirth, M. (2005). Water vapor heterogeneity related to tropopause folds over the North Atlantic revealed by airborne water vapor differential absorption lidar. *Journal of Geophysical Research*, 110(3), 1–17. https://doi.org/10.1029/2004JD004957

Forster, P. M. D. E., & Shine, K. P. (1999). Stratospheric water vapour changes as a possible contributor to observed stratospheric cooling. Geophysical Research Letters, 26(21), 3309–3312. https://doi.org/10.1029/1999gl010487

Forster, P. M. D. E., & Shine, K. P. (2002). Assessing the climate impact of trends in stratospheric water vapor. *Geophysical Research Letters*, 29(6), 10. https://doi.org/10.1029/2001g1013909

Froidevaux, L., Anderson, J., Wang, H.-J., Fuller, R. A., Schwartz, M. J., Santee, M. L., et al. (2015). Global ozone chemistry and related trace gas data records for the stratosphere (gozcards): Methodology and sample results with a focus on hcl, h<sub>2</sub>o, and o<sub>3</sub>. Atmospheric Chemistry and Physics, 15(18), 10471–10507. https://doi.org/10.5194/acp-15-10471-2015

Froidevaux, L., Kinnison, D. E., Wang, R., Anderson, J., & Fuller, R. A. (2019). Evaluation of CESM1 (WACCM) free-running and specified dynamics atmospheric composition simulations using global multispecies satellite data records. *Atmospheric Chemistry and Physics*, 19(7), 4783–4821. https://doi.org/10.5194/acp-19-4783-2019

Fu, Q., Solomon, S., Pahlavan, H. A., & Lin, P. (2019). Observed changes in Brewer-Dobson circulation for 1980–2018. Environmental Research Letters, 14(11), 114026. https://doi.org/10.1088/1748-9326/ab4de7

Fueglistaler, S., Dessler, A. E., Dunkerton, T. J., Folkins, I., Fu, Q., & Mote, P. W. (2009). Tropical tropopause layer. *Reviews of Geophysics*, 47(1), RG1004. https://doi.org/10.1029/2008rg000267

Fueglistaler, S., & Haynes, P. H. (2005). Control of interannual and longer-term variability of stratospheric water vapor. *Journal of Geophysical Research*, 110(D24), D24108. https://doi.org/10.1029/2005jd006019

YU ET AL. 15 of 18



- Garcia, R. R., Marsh, D. R., Kinnison, D. E., Boville, B. A., & Sassi, F. (2007). Simulation of secular trends in the middle atmosphere, 1950–2003. Journal of Geophysical Research, 112(D9), D09301. https://doi.org/10.1029/2006JD007485
- Garcia, R. R., & Randel, W. J. (2008). Acceleration of the Brewer-Dobson circulation due to increases in greenhouse gases. *Journal of the Atmospheric Sciences*, 65(8), 2731–2739. https://doi.org/10.1175/2008JAS2712.1
- Garfinkel, C. I., Gordon, A., Oman, L. D., Li, F., Davis, S., & Pawson, S. (2018). Nonlinear response of tropical lower-stratospheric temperature and water vapor to ENSO. Atmospheric Chemistry and Physics, 18(7), 4597–4615. https://doi.org/10.5194/acp-18-4597-2018
- Garfinkel, C. I., Harari, O., Ziskin, S., Rao, J., Morgenstern, O., Zeng, G., et al. (2020). Influence of ENSO on entry stratospheric water vapor in coupled chemistry-ocean CCMI and CMIP6 models. Atmospheric Chemistry and Physics, 21(5), 1–23. https://doi.org/10.5194/acp-2020-801
- Garfinkel, C. I., Hurwitz, M. M., Oman, L. D., & Waugh, D. W. (2013). Contrasting effects of Central Pacific and Eastern Pacific El Niño on stratospheric water vapor. Geophysical Research Letters, 40(15), 4115–4120. https://doi.org/10.1002/grl.50677
- Geller, M. A., Zhou, X., & Zhang, M. (2002). Simulations of the interannual variability of stratospheric water vapor. *Journal of the Atmospheric Sciences*, 59(6), 1076–1085.
- Gettelman, A., Birner, T., Eyring, V., Akiyoshi, H., Bekki, S., Brühl, C., et al. (2009). The tropical tropopause layer 1960–2100. Atmospheric Chemistry and Physics, 9(5), 1621–1637. https://doi.org/10.3929/ethz-b-000157190
- Gettelman, A., Hegglin, M. I., Son, S. W., Kim, J., Fujiwara, M., Birner, T., et al. (2010). Multimodel assessment of the upper troposphere and lower stratosphere: Tropics and global trends. *Journal of Geophysical Research*, 115(20), D00M08. https://doi.org/10.1029/2009JD013638
- Gettelman, A., Mills, M. J., Kinnison, D. E., Garcia, R. R., Smith, A. K., Marsh, D. R., et al. (2019). The whole atmosphere community climate model version 6 (WACCM6). *Journal of Geophysical Research: Atmospheres*, 124(23), 12380–12403. https://doi.org/10.1029/2019JD030943
- Gunson, M. R., Farmer, C. B., Norton, R. H., Zander, R., Rinsland, C. P., Shaw, J. H., & Gao, B. (1990). Measurements of CH<sub>4</sub>, N<sub>2</sub>O, CO, H<sub>2</sub>O, and O<sub>3</sub> in the middle atmosphere by the atmospheric trace molecule spectroscopy experiment on spacelab 3. *Journal of Geophysical Research*, 95(D9), 13867. https://doi.org/10.1029/id095id09p13867
- Hall, T. M., & Plumb, R. A. (1994). Age as a diagnostic of stratospheric transport. Journal of Geophysical Research, 99(D1), 1059–1070. https://doi.org/10.1029/93JD03192
- Hansen, A. R., & Robinson, G. D. (1989). Water vapor and methane in the upper stratosphere: An examination of some of the nimbus 7 measurements. *Journal of Geophysical Research*, 94(D6), 8474–8484. https://doi.org/10.1029/JD094iD06p08474
- Hegglin, M. I., Plummer, D. A., Shepherd, T. G., Scinocca, J. F., Anderson, J., Froidevaux, L., et al. (2014). Vertical structure of stratospheric water vapour trends derived from merged satellite data. Nature Geoscience, 7(10), 768–776. https://doi.org/10.1038/NGEO2236
- Hervig, M. E., Berger, U., & Siskind, D. E. (2016). Decadal variability in PMCs and implications for changing temperature and water vapor in the upper mesosphere. *Journal of Geophysical Research: Atmospheres*, 121(5), 2383–2392. https://doi.org/10.1002/2015JD024439
- Hurst, D. F., Oltmans, S. J., Vömel, H., Rosenlof, K. H., Davis, S. M., Ray, E. A., et al. (2011). Stratospheric water vapor trends over Boulder, Colorado: Analysis of the 30 year Boulder record. *Journal of Geophysical Research*, 116(2), D02306. https://doi.org/10.1029/2010JD015065
- Hurst, D. F., Read, W. G., Vömel, H., Selkirk, H. B., Rosenlof, K. H., Davis, S. M., et al. (2016). Recent divergences in stratospheric water vapor measurements by frost point hygrometers and the aura microwave limb sounder. *Atmospheric Measurement Techniques*, 9(9), 4447–4457. https://doi.org/10.5194/amt-9-4447-2016
- Johansson, E., Devasthale, A., L'Ecuyer, T., Ekman, A. M., & Tjernström, M. (2015). The vertical structure of cloud radiative heating over the Indian subcontinent during summer monsoon. Atmospheric Chemistry and Physics, 15(20), 11557–11570. https://doi.org/10.5194/ acp-15-11557-2015
- Jones, R. L., Pyle, J. A., Harries, J. E., Zavody, A. M., Russell, J. M., & Gille, J. C. (1986). The water vapour budget of the stratosphere studied using LIMS and SAMS satellite data. *Quarterly Journal of the Royal Meteorological Society*, 112(474), 1127–1143. https://doi.org/10.1002/qj.49711247412
- Kirk-Davidoff, D. B., Hintsa, E. J., Anderson, J. G., & Keith, D. W. (1999). The effect of climate change on ozone depletion through changes in stratospheric water vapour. *Nature*, 402(6760), 399–401. https://doi.org/10.1038/46521
- Kley, D., Russell, J., & Phillips, C. (2000). SPARC assessment of upper tropospheric and stratospheric water vapour (Tech. Rep.). Retrieved from https://www.atmosp.physics.utoronto.ca/SPARC/News16/16
- Lambert, A., Read, W. G., Livesey, N. J., Santee, M. L., Manney, G. L., Froidevaux, L., et al. (2007). Validation of the Aura Microwave Limb Sounder middle atmosphere water vapor and nitrous oxide measurements. *Journal of Geophysical Research*, 112(24), 24–36. https://doi. org/10.1029/2007JD008724
- le Texier, H., Solomon, S., & Garcia, R. R. (1988). The role of molecular hydrogen and methane oxidation in the water vapour budget of the stratosphere. *Quarterly Journal of the Royal Meteorological Society*, 114(480), 281–295. https://doi.org/10.1002/QJ.49711448002
- Li, F., Newman, P., Pawson, S., & Perlwitz, J. (2018). Effects of greenhouse gas increase and stratospheric ozone depletion on stratospheric mean age of air in 1960–2010. *Journal of Geophysical Research: Atmospheres*, 123(4), 2098–2110. https://doi.org/10.1002/2017JD027562
- Lin, S. J. (2004). A "vertically Lagrangian" finite-volume dynamical core for global models. Monthly Weather Review, 132(10), 2293–2307. https://doi.org/10.1175/1520-0493(2004)132<2293;avlfdc>2.0.co;2
- Liu, Z., Kar, J., Zeng, S., Tackett, J., Vaughan, M., Avery, M., et al. (2019). Discriminating between clouds and aerosols in the CALIOP version 4.1 data products. *Atmospheric Measurement Techniques*, 12(1), 703–734. https://doi.org/10.5194/amt-12-703-2019
- Livesey, N. J., Read, W., Lambert, A., Cofield, R., Cuddy, D., Froidevaux, L., et al. (2020). Earth observing system (EOS) aura microwave limb sounder (MLS) description document. (Tech. Rep.).
- Livesey, N. J., Read, W. G., Froidevaux, L., Lambert, A., Santee, M. L., Schwartz, M. J., et al. (2021). Investigation and amelioration of long-term instrumental drifts in water vapor and nitrous oxide measurements from the aura microwave limb sounder (MLS) and their implications for studies of variability and trends. *Atmospheric Chemistry and Physics*, 21(20), 15409–15430. https://doi.org/10.5194/ACP-21-15409-2021
- Lossow, S., Hurst, D. F., Rosenlof, K. H., Stiller, G. P., Von Clarmann, T., Brinkop, S., et al. (2018). Trend differences in lower stratospheric water vapour between boulder and the zonal mean and their role in understanding fundamental observational discrepancies. Atmospheric Chemistry and Physics, 18(11), 8331–8351. https://doi.org/10.5194/acp-18-8331-2018
- Lübken, F.-J., Berger, U., & Baumgarten, G. (2018). On the anthropogenic impact on long-term evolution of noctilucent clouds. *Geophysical Research Letters*, 45(13), 6681–6689, https://doi.org/10.1029/2018GL077719
- Marsh, D. R., Mills, M. J., Kinnison, D. E., Lamarque, J.-F., Calvo, N., & Polvani, L. M. (2013). Climate change from 1850 to 2005 simulated in CESM1(WACCM). *Journal of Climate*, 26(19), 7372–7391. https://doi.org/10.1175/JCLI-D-12-00558.1
- Maycock, A. C., Joshi, M. M., Shine, K. P., Davis, S. M., & Rosenlof, K. H. (2014). The potential impact of changes in lower stratospheric water vapour on stratospheric temperatures over the past 30 years. *Quarterly Journal of the Royal Meteorological Society*, 140(684), 2176–2185. https://doi.org/10.1002/qj.2287
- Maycock, A. C., Joshi, M. M., Shine, K. P., & Scaife, A. A. (2013). The circulation response to idealized changes in stratospheric water vapor. Journal of Climate, 26(2), 545–561. https://doi.org/10.1175/JCLI-D-12-00155.1

YU ET AL. 16 of 18



- Meinshausen, M., Vogel, E., Nauels, A., Lorbacher, K., Meinshausen, N., Etheridge, D. M., et al. (2017). Historical greenhouse gas concentrations for climate modelling (CMIP6). Geoscientific Model Development, 10(5), 2057–2116. https://doi.org/10.5194/gmd-10-2057-2017
- Molod, A., Takacs, L., Suarez, M., & Bacmeister, J. (2015). Development of the GEOS-5 atmospheric general circulation model: Evolution from MERRA to MERRA2. Geoscientific Model Development, 8(5), 1339–1356. https://doi.org/10.5194/GMD-8-1339-2015
- Morgenstern, O., Stone, K. A., Schofield, R., Akiyoshi, H., Yamashita, Y., Kinnison, D. E., et al. (2018). Ozone sensitivity to varying green-house gases and ozone-depleting substances in CCMI-1 simulations. Atmospheric Chemistry and Physics, 18(2), 1091–1114. https://doi.org/10.5194/ACP-18-1091-2018
- Mote, P. W., Rosenlof, K. H., Mcintyre, E., Carr, E. S., Gille, J. C., Holton, R., et al. (1996). An atmospheric tape recorder. *Journal of Geophysical Research*, 101(95), 3989–4006. https://doi.org/10.1029/95jd03422
- Nedoluha, G. E., Michael Gomez, R., Allen, D. R., Lambert, A., Boone, C., & Stiller, G. (2013). Variations in middle atmospheric water vapor from 2004 to 2013. *Journal of Geophysical Research: Atmospheres*, 118(19), 11–285. https://doi.org/10.1002/jgrd.50834
- Newman, P. A., Daniel, J. S., Waugh, D. W., & Nash, E. R. (2007). A new formulation of equivalent effective stratospheric chlorine (EESC). Atmospheric Chemistry and Physics, 7(17), 4537–4552. https://doi.org/10.5194/ACP-7-4537-2007
- Noël, S., Weigel, K., Bramstedt, K., Rozanov, A., Weber, M., Bovensmann, H., & Burrows, J. P. (2018). Water vapour and methane coupling in the stratosphere observed using sciamachy solar occultation measurements. Atmospheric Chemistry and Physics, 18(7), 4463–4476. https://doi.org/10.5194/acp-18-4463-2018
- Oberländer-Hayn, S., Meul, S., Langematz, U., Abalichin, J., & Haenel, F. (2015). A chemistry-climate model study of past changes in the Brewer-Dobson circulation. *Journal of Geophysical Research: Atmospheres*, 120(14), 6742–6757. https://doi.org/10.1002/2014JD022843
- Oman, L. D., Waugh, D. W., Pawson, S., Stolarski, R. S., & Nielsen, J. E. (2008). Understanding the changes of stratospheric water vapor in coupled chemistry–climate model simulations. *Journal of the Atmospheric Sciences*, 65(10), 3278–3291. https://doi.org/10.1175/2008JAS2696.1
- Ploeger, F., Diallo, M., Charlesworth, E., Konopka, P., Legras, B., Laube, J. C., et al. (2021). The stratospheric Brewer-Dobson circulation inferred from age of air in the ERA5 reanalysis. *Atmospheric Chemistry and Physics*, 21(11), 8393–8412. https://doi.org/10.5194/acp-21-8393-2021
- Ploeger, F., Günther, G., Konopka, P., Fueglistaler, S., Müller, R., Hoppe, C., et al. (2013). Horizontal water vapor transport in the lower stratosphere from subtropics to high latitudes during boreal summer. *Journal of Geophysical Research: Atmospheres*, 118(14), 8111–8127. https://doi.org/10.1002/jgrd.50636
- Ploeger, F., Legras, B., Charlesworth, E., Yan, X., Diallo, M., Konopka, P., et al. (2019). How robust are stratospheric age of air trends from different reanalyses? Atmospheric Chemistry and Physics, 19(9), 6085–6105. https://doi.org/10.5194/ACP-19-6085-2019
- Polvani, L. M., Abalos, M., Garcia, R., Kinnison, D., & Randel, W. J. (2018). Significant weakening of Brewer-Dobson circulation trends over the 21st century as a consequence of the montreal protocol. Geophysical Research Letters, 45(1), 401–409. https://doi.org/10.1002/2017GL075345
- Polvani, L. M., Wang, L., Abalos, M., Butchart, N., Chipperfield, M. P., Dameris, M., et al. (2019). Large impacts, past and future, of ozone-depleting substances on Brewer-Dobson circulation trends: A multimodel assessment. *Journal of Geophysical Research: Atmospheres*, 124(13), 6669–6680. https://doi.org/10.1029/2018JD029516
- Randel, W. J., & Park, M. (2019). Diagnosing observed stratospheric water vapor relationships to the cold point tropical tropopause. *Journal of Geophysical Research: Atmospheres*, 124(13), 7018–7033. https://doi.org/10.1029/2019JD030648
- Randel, W. J., Wu, F., Oltmans, S. J., Rosenlof, K., & Nedoluha, G. E. (2004). Interannual changes of stratospheric water vapor and correlations with tropical tropopause temperatures. *Journal of the Atmospheric Sciences*, 61(17), 2133–2148. https://doi. org/10.1175/1520-0469(2004)061<2133:icoswv>2.0.co;2
- Randel, W. J., Wu, F., Vömel, H., Nedoluha, G. E., & Forster, P. M. D. E. (2006). Decreases in stratospheric water vapor after 2001: Links to changes in the tropical tropopause and the Brewer-Dobson circulation. *Journal of Geophysical Research*, 111(D12), D12312. https://doi.org/10.1029/2005JD006744
- Ray, E. A., Moore, F. L., Rosenlof, K. H., Davis, S. M., Boenisch, H., Morgenstern, O., et al. (2010). Evidence for changes in stratospheric transport and mixing over the past three decades based on multiple data sets and tropical leaky pipe analysis. *Journal of Geophysical Research*, 115(D21), D21304. https://doi.org/10.1029/2010jd014206
- Read, W. G., Lambert, A., Bacmeister, J., Cofield, R. E., Christensen, L. E., Cuddy, D. T., et al. (2007). Aura microwave limb sounder upper tropospheric and lower stratospheric H<sub>2</sub>O and relative humidity with respect to ice validation. *Journal of Geophysical Research*, 112(24), D24S35, https://doi.org/10.1029/2007JD008752
- Remsberg, E. E., Marshall, B. T., Garcia-Comas, M., Krueger, D., Lingenfelser, G. S., Martin-Torres, J., et al. (2008). Assessment of the quality of the version 1.07 temperature-versus-pressure profiles of the middle atmosphere from TIMED/SABER. *Journal of Geophysical Research*, 113(D17), 17101. https://doi.org/10.1029/2008JD010013
- Rezac, L., Yue, J., Yongxiao, J., Russell, J. M., III., Garcia, R., López-Puertas, M., & Mlynczak, M. G. (2018). On long-Term SABER CO<sub>2</sub> Trends and Effects Due to Nonuniform Space and Time Sampling. *Journal of Geophysical Research: Space Physics*, 123(9), 7958–7967. https://doi.org/10.1029/2018ja025892
- Rind, D., & Lonergan, P. (1995). Modeled impacts of stratospheric ozone and water vapor perturbations with implications for high-speed civil transport aircraft. *Journal of Geophysical Research*, 100(D4), 7381–7396. https://doi.org/10.1029/95JD00196
- Rong, P., Russell, J. M. I., Marshall, B. T., Gordley, L. L., Mlynczak, M. G., & Walker, K. A. (2019). Validation of water vapor measured by SABER on the timed satellite. *Journal of Atmospheric and Solar-Terrestrial Physics*, 194, 105099. https://doi.org/10.1016/j.jastp.2019.105099
- Rosenlof, K. H. (2002). Transport changes inferred from HALOE water and methane measurements. *Journal of the Meteorological Society of Japan*, 80(4 B), 831–848. https://doi.org/10.2151/jmsj.80.831
- Rosenlof, K. H., Oltmans, S., Kley, D., Russell, J., III., Chiou, E.-W., Chu, W., et al. (2001). Stratospheric water vapor increases over the past half-century. *Geophysical Research Letters*, 28(7), 1195–1198. https://doi.org/10.1029/2000gl012502
- Rosenlof, K. H., & Reid, G. C. (2008). Trends in the temperature and water vapor content of the tropical lower stratosphere: Sea surface connection. *Journal of Geophysical Research*, 113(D6), 6107. https://doi.org/10.1029/2007JD009109
- Russell, J. M. I., Gordley, L. L., Park, J. H., Drayson, R., Hesketh, W. D., Cicerone, R. J., et al. (1993). The halogen occultation experiment. Journal of Geophysical Research, 98(D6), 10777–10797. https://doi.org/10.1029/93jd00799
- Russell, J. M. I., Mlynczak, M. G., Gordley, L. L., Tansock, J. J., Jr., & Esplin, R. W. (1999). Overview of the saber experiment and preliminary calibration results. In (Vol. 3756, p. 277). International Society for Optics and Photonics. https://doi.org/10.1117/12.366382
- Russell, J. M. I., Rong, P., Hervig, M. E., Siskind, D. E., Stevens, M. H., Bailey, S. M., & Gumbel, J. (2014). Analysis of northern midlatitude noctilucent cloud occurrences using satellite data and modeling. *Journal of Geophysical Research: Atmospheres*, 119(6), 3238–3250. https://doi.org/10.1002/2013JD021017
- Scaife, A. A., Butchart, N., Jackson, D. R., & Swinbank, R. (2003). Can changes in enso activity help to explain increasing stratospheric water vapor? Geophysical Research Letters, 30(17), 1880. https://doi.org/10.1029/2003gl017591

YU ET AL. 17 of 18



- Schoeberl, M. R., Dessler, A. E., Wang, T., Avery, M. A., & Jensen, E. J. (2014). Cloud formation, convection, and stratospheric dehydration. Earth and Space Science, 1(1), 1–17. https://doi.org/10.1002/2014EA000014
- Schwartz, M. J., Read, W. G., Santee, M. L., Livesey, N. J., Froidevaux, L., Lambert, A., & Manney, G. L. (2013). Convectively injected water vapor in the North American summer lowermost stratosphere. *Geophysical Research Letters*, 40(10), 2316–2321. https://doi.org/10.1002/grl.50421
- Sherwood, S. C., & Dessler, A. E. (2000). On the control of stratospheric humidity. Geophysical Research Letters, 27(16), 2513–2516. https://doi.org/10.1029/2000g1011438
- Sherwood, S. C., Minnis, P., & McGill, M. (2004). Deep convective cloud-top heights and their thermodynamic control during crystal-face. *Journal of Geophysical Research*, 109(20), 1–11. https://doi.org/10.1029/2004JD004811
- Shindell, D. T. (2001). Climate and ozone response to increased stratospheric water vapor. *Geophysical Research Letters*, 28(8), 1551–1554. https://doi.org/10.1029/1999GL011197
- Smith, C. A., Haigh, J. D., & Toumi, R. (2001). Radiative forcing due to trends in stratospheric water vapour. Geophysical Research Letters, 28(1), 179–182. https://doi.org/10.1029/2000GL011846
- Solomon, S., Ivy, D. J., Kinnison, D., Mills, M. J., Neely, R. R., III., & Schmidt, A. (2016). Emergence of healing in the Antarctic ozone layer. Science, 353(6296), 269–274. https://doi.org/10.1126/science.aae0061
- Solomon, S., Rosenlof, K. H., Portmann, R. W., Daniel, J. S., Davis, S. M., Sanford, T. J., & Plattner, G.-K. (2010). Contributions of stratospheric water vapor to decadal changes in the rate of global warming. *Science*, 327(5970), 1219–1223. https://doi.org/10.1126/science.1182488
- water vapor to decadal changes in the rate of global warming. Science, 327(5970), 1219–1223. https://doi.org/10.1126/science.1182488
  Tao, M., Konopka, P., Ploeger, F., Riese, M., Müller, R., & Volk, C. M. (2015). Impact of stratospheric major warmings and the quasi-biennial oscil-
- lation on the variability of stratospheric water vapor. *Geophysical Research Letters*, 42(11), 4599–4607. https://doi.org/10.1002/2015gl064443
  Thomas, G. E. (2003). Are noctilucent clouds harbingers of global change in the middle atmosphere? *Advances in Space Research*, 32(9), 1737–1746. https://doi.org/10.1016/S0273-1177(03)90470-4
- Tiao, G. C., Reinsel, G. C., Xu, D., Pedrick, J., Zhu, X., Miller, A., et al. (1990). Effects of autocorrelation and temporal sampling schemes on estimates of trend and spatial correlation. *Journal of Geophysical Research*, 95(D12), 20507–20517. https://doi.org/10.1029/jd095id12p20507
- Wang, X., Dessler, A. E., Schoeberl, M. R., Yu, W., & Wang, T. (2019). Impact of convectively lofted ice on the seasonal cycle of water vapor in the tropical tropopause layer. *Atmospheric Chemistry and Physics*, 19(23), 14621–14636, https://doi.org/10.5194/acp-19-14621-2019
- Waters, J. W., Froidevaux, L., Harwood, R. S., Jarnot, R. F., Pickett, H. M., Read, W. G., et al. (2006). The Earth observing system microwave limb sounder (EOS MLS) on the aura satellite. *IEEE Transactions on Geoscience and Remote Sensing*, 44(5), 1075–1092. https://doi.org/10.1109/TGRS.2006.873771
- Wrotny, J. E., Nedoluha, G. E., Boone, C., Stiller, G. P., & McCormack, J. P. (2010). Total hydrogen budget of the equatorial upper stratosphere. Journal of Geophysical Research, 115(D4), D04302. https://doi.org/10.1029/2009jd012135
- Ye, H., Dessler, A. E., & Yu, W. (2018). Effects of convective ice evaporation on interannual variability of tropical tropopause layer water vapor. Atmospheric Chemistry and Physics, 18(7), 4425–4437. https://doi.org/10.5194/acp-18-4425-2018
- Yu, W., Dessler, A. E., Park, M., & Jensen, E. J. (2020). Influence of convection on stratospheric water vapor in the North American monsoon region. Atmospheric Chemistry and Physics, 20(20), 12153–12161. https://doi.org/10.5194/acp-20-12153-2020
- Yu, W., Garcia, R., Yue, J., Russell, J., & Mlynczak, M. (2022a). A merged satellite data from SABER, MLS, and HALOE [Dataset]. Zenodo. https://doi.org/10.5281/ZENODO.6308969
- Yu, W., Garcia, R., Yue, J., Russell, J., & Mlynczak, M. (2022b). Code for "Variability of water vapor in the tropical middle atmosphere observed from satellites and interpreted using SD-WACCM simulations". Zenodo. https://doi.org/10.5281/ZENODO.6774398
- Yue, J., Russell, J., Jian, Y., Rezac, L., Garcia, R., Lõpez-Puertas, M., & Mlynczak, M. G. (2015). Increasing carbon dioxide concentration in the upper atmosphere observed by SABER. *Geophysical Research Letters*, 42(17), 7194–7199. https://doi.org/10.1002/2015GL064696
- Yue, J., Russell, J. M. I., Gan, Q., Wang, T., Rong, P., Garcia, R., & Mlynczak, M. (2019). Increasing water vapor in the stratosphere and mesosphere after 2002. Geophysical Research Letters, 46(22), 13452–13460. https://doi.org/10.1029/2019GL084973
- Zahn, A., Christner, E., Van Velthoven, P. F., Rauthe-Schöch, A., & Brenninkmeijer, C. A. (2014). Processes controlling water vapor in the upper troposphere/lowermost stratosphere: An analysis of 8years of monthly measurements by the IAGOS-CARIBIC observatory. *Journal of Geophysical Research*, 119(19), 11505–11525. https://doi.org/10.1002/2014JD021687

YU ET AL. 18 of 18